NRL Report 6487

NRL Terrain Clutter Study Phase I

N. W. GUINARD, J. T. RANSONE, JR., M. B. LAING, AND L. E. HEARTON

Wave Propagation Branch
Electronics Division

May 10, 1967

NAVAL RESEARCH LABORATORY
Washington, D.C.

9

CONTENTS

ABSTRACT

The first phase of a terrain-clutter study has been completed at NRL, utilizing the four-frequency radar system installed in a WV2-128324 (Super Constellation) aircraft. This system is capable of transmitting and receiving four frequencies (P, L, C, and X) consecutively with a choice of horizontal, vertical, and alternating polarizations. The returns are gated at a fixed range and analyzed in a digital computer. Absolute clutter measurements have been taken over both Canadian and American sites at angles of incidence of 10 degrees or less. Two parameters have been measured. The first is the normalized radar cross section in terms of the 10, 50 (median), and 90 percentile values of its distribution, while the second is the fluctuation power spectrum of the coherent radar return signal. Two types of statistical processes have been determined from the cross-section data; one follows a Rayleigh distribution between 10 and 90 percentile values, and one departs radically from this distribution. The energy in the fluctuation power spectrum has been estimated in frequency bands whose spacing is determined by the transmitted frequency, e.g., 2 cps at P band through 10 cps at X band. The root mean square deviations of the estimates indicate likewise a Rayleigh behavior for certain bands and a radical departure from this behavior. In this case, the radical departure is identified as a Ricean (signal plus noise) distribution produced by strongly reflecting point targets in the illuminated area. A statistical model for terrain clutter is proposed which will enable the phenomenon disclosed by the study to be simulated based upon the optical analysis of Synthetic Aperture Radar Maps.

PROBLEM STATUS

This is a final report on this phase of the problem; work on other phases is continuing.

AUTHORIZATION

NRL Problem R07-02
AF MIPR AS-5-64

Manuscript submitted September 7, 1966

NRL TERRAIN CLUTTER STUDY
PHASE I

INTRODUCTION

The Naval Research Laboratory is currently conducting a clutter measurement program for the Research and Technology Division, Systems Engineering Group, Wright-Patterson AFB, Ohio. This report is a summary of results and data accumulated during the first phase of the program, covering 18 months of effort, and is offered in lieu of bimonthly reports four, five, and six. During the course of the program to date, three major reports (1, 2, 3) were produced which contained large quantities of data and analyses pertinent to them, which were circulated to workers in the field.

The purpose of the present work as contained in the MIPR AS-5-64 is to "contribute technical data to establish clutter models ... that can be used for theoretical evaluation of various rejection techniques ..." To achieve this purpose, data were collected by personnel in the NRL instrumented aircraft WV-128324 (Fig. 1). The initial objective of the study was to acquire data on four frequencies and two polarizations, at low angles of incidence (less than 10 degrees) over both American and Canadian terrain. The data collected were to be processed to determine both the amplitude distribution and power spectra of the clutter return. Due to operational difficulty in acquiring spectral data, early flights yielded only partial success; however, by July 1965 most of these difficulties were overcome, and the complete set of signals was recorded. Table 1 gives a listing of the flights on which the majority of the data in this report were taken, with comments on the nature of the data acquired.

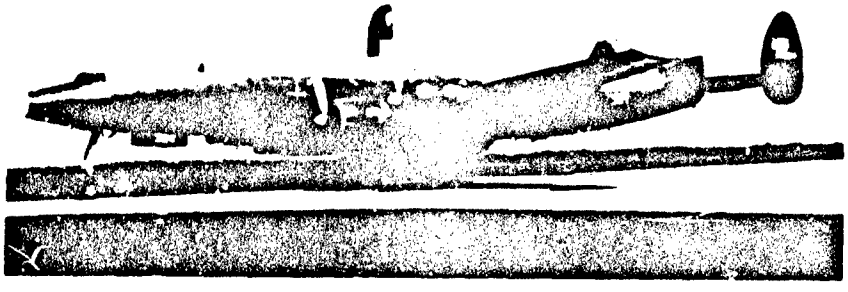

Fig. 1 - Radar-instrumented Super-Constellation NRL Aircraft used in terrain-clutter studies

The major portion of the instrumentation carried by the NRL aircraft is the four-frequency (4F) radar system, a research radar which is capable of transmitting coherently an eight-pulse sequence of the form P_H, X_H, L_H, C_H, P_L, X_L, L_L, C_L, where

Table 1
Flight Summary

Date	Flight Path	Elevation Angle (degrees)	Polarization	Frequency	Object
Sept. 8, 64	Goose Bay, Labrador to Winnipeg	4–1/2–9	VV, HH, VH, HV	X band	Cross Section
Sept. 12, 64	Nebraska, Wyoming, Utah	5–7	VV, HH, VH, HV	X band	Cross Section
Sept. 13, 64	Milford, Utah to So. Arizona	3–5	VV, HH, VH, HV	X band	Cross Section
Sept. 16, 64	Dyersburg, Tenn. to West Va.	3–1/2–7	VV, HH, VH, HV	X band	Cross Section
Dec. 10, 64	Eastern Shore, Md.	4	VV, HH	X and C band	Spectra
July 2, 65	Iowa, Ill., Ind., Ohio (Denver flight)	8	VV, HH, VH, HV	P, L, C, X bands	Cross Section and Spectra

the subscripts refer to the transmitted polarization The repetition rate of the sequence is variable, with a maximum rate of 788 per second, so that, for example, the prf associated with the P_H transmission is 788 pps.

A simplified block diagram of the receiving system is shown in Fig. 2. For each pulse transmission, the horizontal and vertical components of the backscatter are separately sensed by the antenna system, converted coherently to i-f, and fed to lin-log and linear i-f amplifier pairs which are designed to preserve amplitude and phase of the envelope of the return respectively. In the logarithmic strip the dynamic range is compressed for easy digitalization, incoherently detected (square law), and used as output to the range-gating and digitalization circuitry. Simultaneously, in the linear strip, the signal is amplified with minimum phase distortion, hard limited to eliminate amplitude variations, coherently detected, and is used as output to the range-gating and digitalization circuitry. The other polarization component is treated in similar fashion. Some question has arisen concerning the effect of the hard-limiting process on the clutter

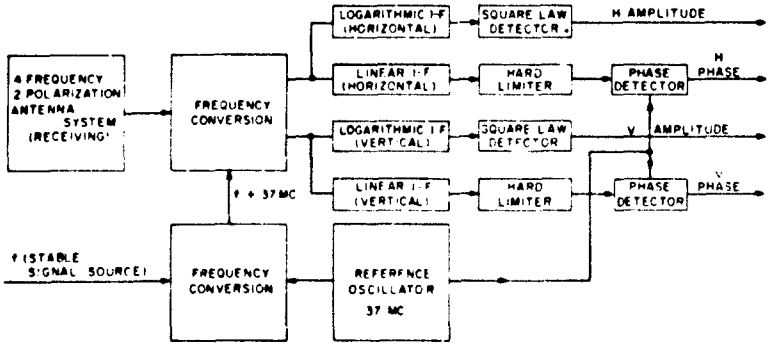

Fig. 2 - Simplified block diagram of four-frequency radar receiving system

spectrum; this will be treated in a later section of the report. For the next pulse transmission, the frequency-conversion unit and the stable signal source are switched to provide the correct signals and circuitry to convert the new frequency/polarization transmission to i-f, and the same lin-log strip system is used for amplification and detection. The common i-f system not only eliminates receiver errors but also simplifies the calibration procedure. A detailed account of the 4F radar system will be found in Appendix A.

A nomenclature has been evolved to describe the various outputs of the system. The letters P, L, C, and X designate the transmissions on frequencies of 428, 1228, 4455, and 8910 Mc respectively. The polarized returns will be symbolized by letter combinations of the form HH, VH, etc., where the first letter denotes the transmitted polarization and the second the received. The frequency-band letters will be used for the amplitude of the return with polarization subscripts, while the phase of the returns will be designated by ϕ with polarization subscripts. It should be noted that for the eight-pulse sequence previously indicated, there are 32 recorded outputs per range gate, producing a data rate of 25 kilowords per second.

The transmitting and receiving antenna system consists of four dual-polarization antennas. These antennas are mounted in pairs back to back. The X- and C-band antennas are mounted side by side, and the beams are colinear and have the same beamwidth, so that they illuminate the same area. L- and P-band antennas are mounted 180 degrees in azimuth from X- and C-band antennas, and are likewise colinear but have different beamwidths, so that the area illuminated by the P-band antenna includes the area illuminated by the L-band antenna. The antenna pairs, while locked in azimuth, are separately trained in elevation from 0 degree (horizontal) to 90 degrees (vertical). The entire array may be scanned through 315 degrees of azimuth, or any portion thereof. Two views of this system are shown in Fig. 3.

Two modes of data collection were employed in the flights listed in Table 1. The first is a searchlight mode, in which the antennas are held at fixed azimuth and elevation angles. These are held relatively constant by stabilization referenced to vertical and magnetic north. The second is a scanning mode, in which the antenna system is sector scanned through a prescribed angle continually for the duration of the run. In both cases, the aircraft is attempting to maintain a constant heading, altitude, and velocity over the desired flight path. The searchlight runs are used primarily to acquire spectral data and amplitude variations along a strip. The scanning runs allow collection of the amplitude variation statistics over a larger area to determine wavelength and angle-of-incidence dependence. In order to describe the nature of the terrain along the flight path, maps have been provided which indicate the geographical area in which the data were taken and the flight path as determined from the aircraft instruments and visual observations. These maps are shown in Figs. 4 through 8. The flight path is shown as a vector labeled with the run number (octal notation). The vector lies along the ground track. The date and run number specify a unique flight path, while time along the path is specified by the relative time clock in the recording system.

The remainder of this report will deal primarily with the data acquired and will attempt to provide sufficient information to enable the reader to utilize the data, within its limitations. In addition, certain generalizations will be made concerning the nature of clutter and the clutter process. Since the primary objective of this program is to implement a clutter model for radar evaluation, a statistical model is proposed which, it is felt, will include both the geographic and reflective properties of the terrain in a manner suitable for computer implementation.

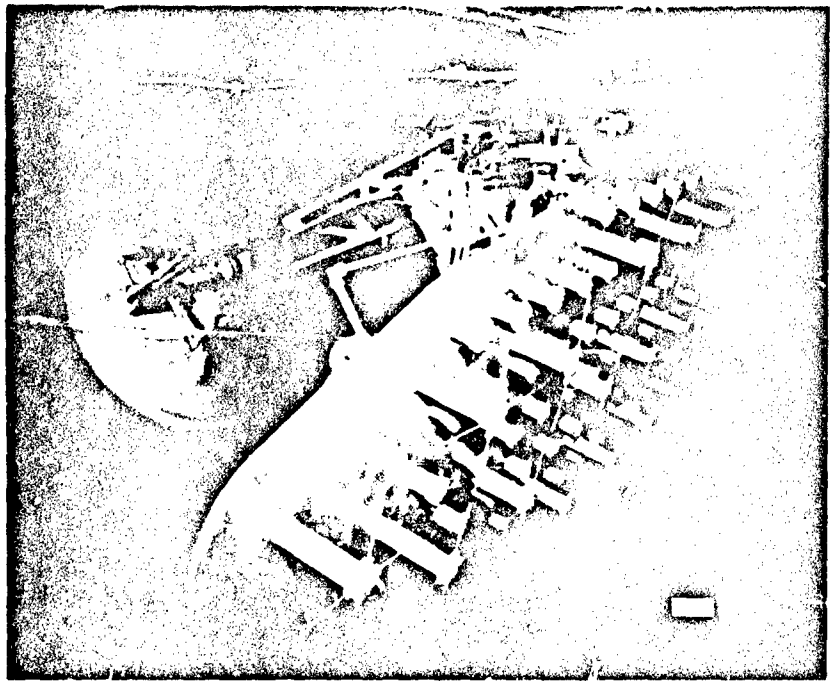

a. L and P band array

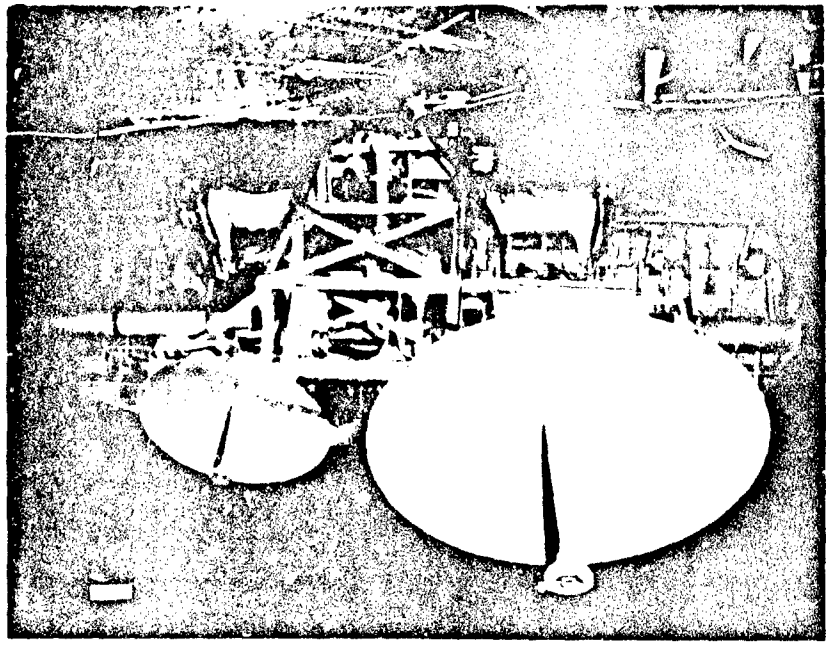

b. X and C dishes

Fig. 3 - Four-frequency antenna system installed in lower radome of aircraft

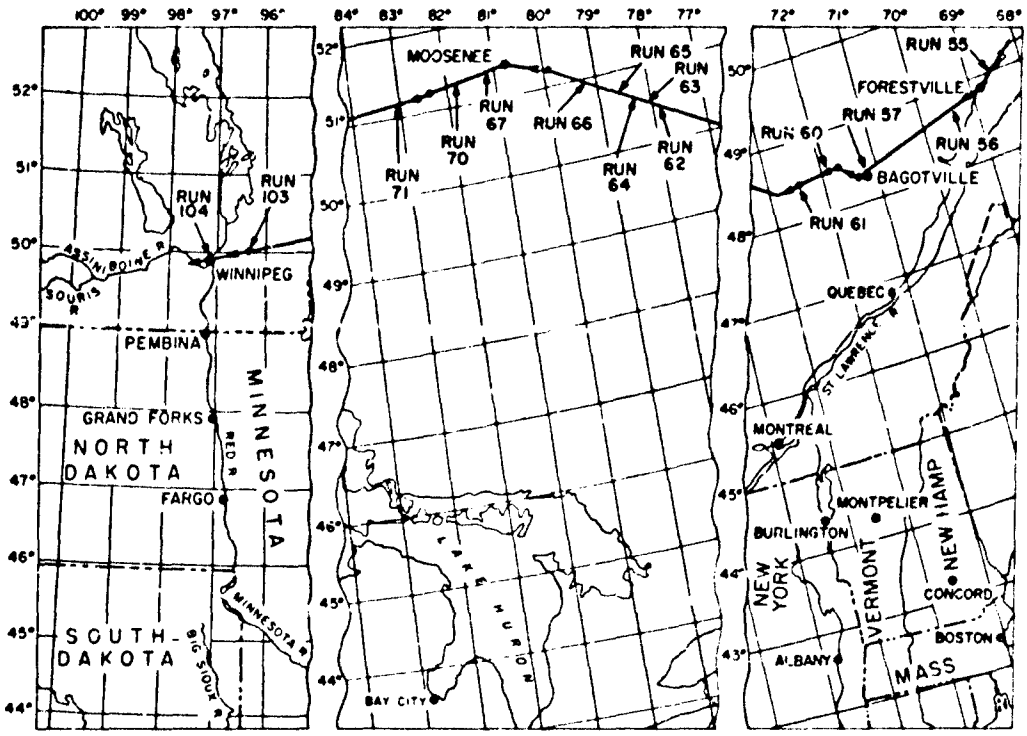

Fig. 4 - Flight path, Sept. 8, 1964, Canada

TERRAIN CLUTTER

Clutter Analysis

Clutter is generally considered, from the standpoint of mathematical tractability, to be the energy scattered back to a radar from a random array of targets of roughly equal cross section. The scatterers are further assumed to be uniformly distributed over the illuminated area and along the flight path. The signal returned is the result of the vector addition (random walk) of the contributions of each scatterer illuminated by the radar. The number of scatterers is assumed sufficiently large to ensure convergence of the statistics. This set of assumptions will be termed the "sandpaper clutter model" for brevity. Fluctuations in the amplitude of the clutter signal arise as the result of several mechanisms: (a) the relative motion of the scatterers with respect to each other (internal motion); (b) variations in the phase of the returns from the various scatterers with respect to the radar because of antenna scanning motion; (c) similar variations produced by platform motion (aircraft velocity); (d) phase shifts induced by error motions, i.e., pitch, roll, and yaw of airframe, velocity variations, etc. The sandpaper model has been analyzed by several scientists and the effects of each of the above mechanisms assessed. Barlow (4) has curve fit a Gaussian spectral shape to internal-motion phase variations by observing the fluctuations of a searchlighting fixed radar. The variance of the distribution is given for various situations, wind-blown leaves, waves, etc. Emerson (5) among others has analyzed the fluctuation spectra produced by antenna and aircraft motions and has developed Gaussian-shaped spectra for their phase variations. The antenna is assumed to be Gaussian in shape, with a standard deviation equal to the

half beamwidth. Due to the statistical independence of the various mechanisms, the form of the clutter spectrum becomes

$$W_c(f) = \frac{1}{2\pi\sigma_c^2} \exp -\left(\frac{f^2}{2\sigma_c^2}\right) \tag{1}$$

where

$$\sigma_c^2 = \sigma_{tm}^2 + \sigma_a^2 + \sigma_{pm}^2 \tag{2}$$

$$\sigma_{tm} = \frac{2v}{\lambda}$$

$$\sigma_a = 0.266 \frac{a \omega^{\alpha}}{\lambda}$$

$$\sigma_{pm} = 0.625 \frac{L \sin \theta}{\lambda} .$$

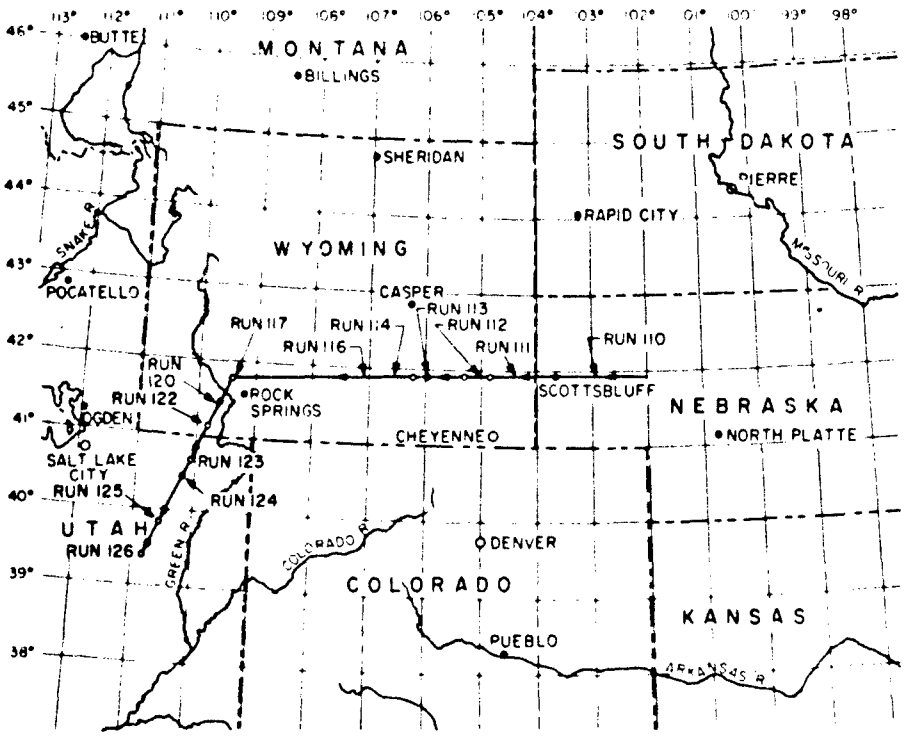

Fig. 5 - Flight path, Sept. 12, 1964, Nebraska to Utah

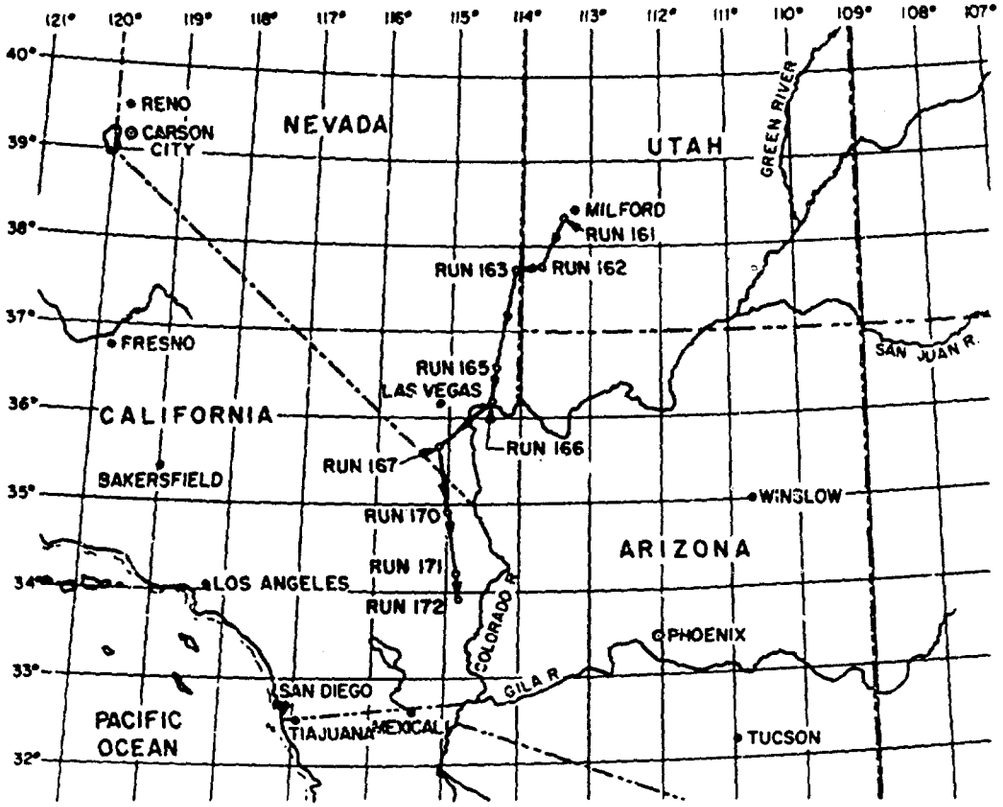

Fig. 6 - Flight path, Sept. 13, 1964, Utah to California

In the above, $W_c(f)$ is the unit clutter power spectrum whose variance is σ_c; σ_{im}, σ_a and σ_{pm} are the standard deviations of the internal motion, scanning, and platform motion spectra respectively; v is the standard deviation of particle velocities in the clutter cell; ψ', the scan rate; v the aircraft velocity; a, the antenna aperture; ψ, the antenna angle measured from ground track; and λ, the wavelength. Therefore, the normalized clutter correlation function of lag τ becomes

$$\phi_c(\tau) = e^{-2(\pi\sigma_c\tau)^2} . \tag{3}$$

Having the spectral distribution and the correlation function of the clutter process, it is only necessary to determine the total distribution of the clutter amplitudes to describe the process completely. The sandpaper model is a form of the two-dimensional random-walk problem, which yields a Rayleigh distribution for the clutter envelope amplitude, V,

$$P(V) = \frac{V}{\sigma_v^2} \exp\left(-\frac{V^2}{2\sigma_v}\right) . \tag{4}$$

where σ_v is the standard deviation of the amplitude. From the radar equation, the clutter cross section S is proportional to V^2, so that

$$P(S) = \frac{1}{\sigma_{AV}} \exp\left(-\frac{S}{\sigma_{av}}\right) . \tag{5}$$

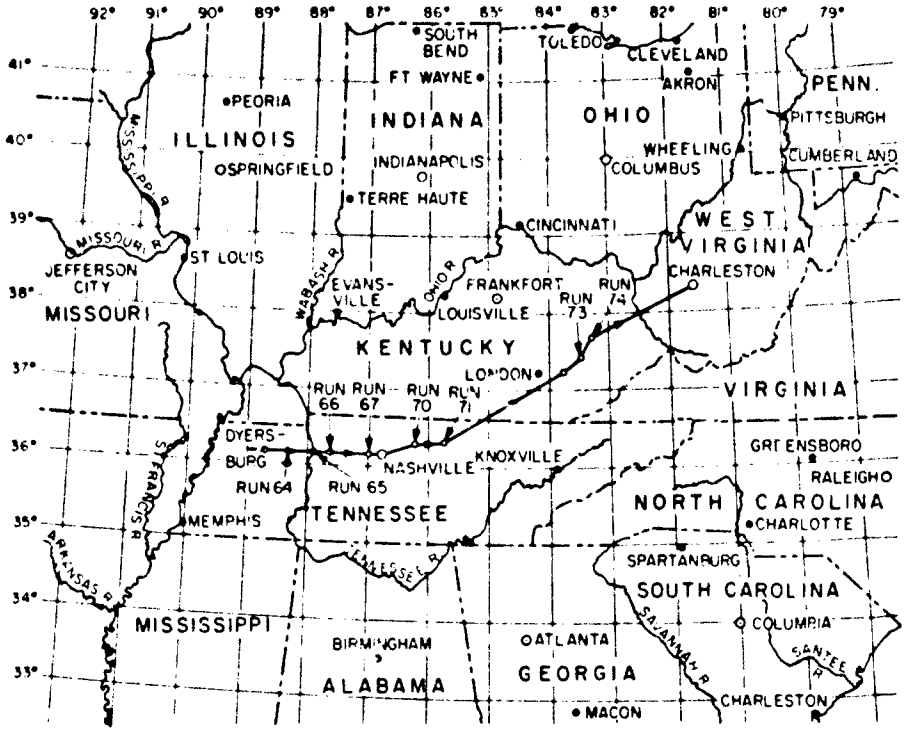

Fig. 7 - Flight path, Sept. 16, 1964, Tennessee to West Virginia

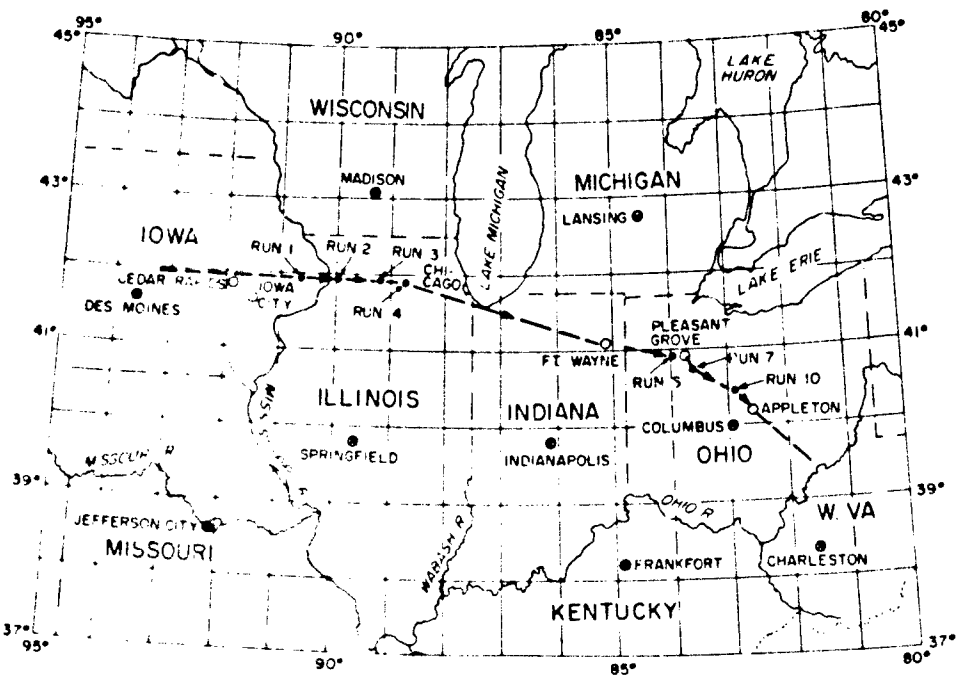

Fig. 8 - Flight path, July 2, 1965, Iowa to Ohio

where the nonrandom radar parameters have been eliminated by normalization. The radar-system parameters and flight geometry, combined with the above description of the clutter process, enable the analyst, at least in theory, to predict the performance of conventional radars. The performance characteristics obtained are strongly influenced by the values used for the variance of the internal motion spectrum and the value used for the terrain cross section, s. Unfortunately, these parameters vary widely over the surface of the earth, and exact measurements are difficult to obtain. For radar systems in which the platform motion spectrum has a small variance, the internal motion spectrum has a strong influence on performance; however, for most airborne systems the platform motion spectrum is sufficiently large to dominate the clutter spectrum, so that the internal-motion spectrum has little influence on performance. In both cases, the spatial variation of the terrain cross section is of primary importance.

The specification of terrain cross section is complicated, since its value depends upon the roughness of the terrain, angle of incidence, wavelength of the incident radiation and its polarization, and the size of the illuminated patch. The cross section is also a function of the azimuth at which the data are taken. This variation is handled in these data by either a tacit assumption of azimuthal symmetry, where a fixed angle is used, or by operationally scanning the antenna of the radar during data collection to integrate azimuthal effects. The following sections will deal with measured values of the cross-section distribution and the clutter power spectrum, both to enable implementation of the sandpaper clutter model and to provide values for analyses where the assumptions of the model, i. e., spectral shape, cross-section distribution, stationarity, etc., are sufficiently imprecise to cause difficulty.

Clutter Cross Section

The basic parameter measured in the amplitude channel of the four-frequency radar is the logarithm of the square of the instantaneous amplitude of the clutter return, quantized to seven-bit precision (128 levels). By suitable calibration, described in Appendix B, an absolute value of the terrain cross section can be achieved. In processing the data, the logarithmic form is preserved and logarithmic axes are used. With these axes the amplitude and the cross section become identical and may be used interchangeably, a point which has caused some confusion in the past. The value of the cross section is given by the radar equation as

$$\sigma = \frac{(4\pi)^3 R^4 P_r}{\lambda^2 G^2(\theta, \psi) P_T} = K\left(\frac{P_r}{P_T}\right), \tag{6}$$

where the radar parameters have the usual significance. The constant K is known from the system parameters, and geometry, and (P_r/P_T) is determined by the calibration procedure. The value of σ, thus obtained, is dependent upon the area illuminated by the radar. To eliminate this dependence, it is standard to compute the normalized cross section, defined as

$$\sigma_0 = \frac{\sigma}{A} \tag{7}$$

where

$$A \cong R\psi_a \frac{\frac{1}{2} c\tau}{\cos\psi} \qquad \text{for small depression angles,}$$

$$A \cong \frac{R^2 \psi_a \theta}{\sin \psi} \qquad \text{for large depression angles.} \tag{8}$$

The raw data which are recorded in flight are processed in a small, general-purpose digital computer (Raytheon 250) in the following manner. A relative scale is established by utilizing the fact that due to quantization of the signal into 128 levels, it is possible to determine the cumulative distribution function by noting the number of signals in a given sample time which exceed each level. The scale is calibrated by adding the appropriate values (in decibels) of t, the illuminated area, sample size, and K to each level, thus yielding the absolute value of σ_0. The level which is exceeded by 50 percent of the pulses in a given sample time is the median value of the distribution, σ_m. This parameter was chosen as characteristic of the distribution rather than the mean to which it is related in a Rayleigh distribution by

$$\sigma_{av} = \sigma_m + 1.6 \text{ db}, \tag{9}$$

since it is less sensitive to errors which are concentrated at the high or low ends of the distribution. The errors at the high-signal end of the distribution are attributable to receiver saturation, while those at the low-signal end are attributable to averaging in the finite-width range gate, and receiver noise. To minimize the gating error, a 30-nanosec gate width is normally used.

For each time sample in a given data run, the entire distribution is computed. Two forms of presentation of the cross-section data will be found in this report. For runs in which the antenna is scanned at constant elevation, the entire distribution of cross sections is given; that is, the total ensemble of range-gate samples over the entire run are distributed and calibrated. The data are presented in tabular form with selected percentile values. Normally, the 100 percentile is the lowest received pulse, while the 0 percentile is the value of the largest pulse in the distribution. Occasionally, the lower end of the distribution will be in the receiver noise. The tables will then commence with the percentile level at the minimum detectable signal.

A sampling of the data taken in this program may be found in Tables 2 through 6. Table 2 lists the operating conditions for the September 1964 flights, while Table 3 lists the cumulative distributions for the various runs. A similar format is used for the Denver data. It is valuable to determine from these data the validity of the assumed Rayleigh envelope distribution. A convenient representation of the closeness of fit of the clutter distribution to the assumed distribution is the plot of data points on Rayleigh paper. Figures 9, 10, and 11 are examples of this representation. The ordinate is the value in decibels of the amplitude level, while the abscissa is the percentage of the samples which exceed that level in a fixed time. The sample size is 1000 pulses, which at 788 pps is 1.27 sec of flight time. Figure 9a shows the nature of the fit which may be obtained. A Rayleigh distribution plotted in this fashion should have a slope equal to that of the theoretical line drawn on the figure. The data shown are roughly parallel to the theoretical line through the middle portion of the plot and depart at the high and low ends for reasons previously stated. Figure 9c shows a radical departure from the assumed distribution. A major attempt will be made in the course of this study to determine the effect on a generalized radar of this departure from Rayleigh upon the probability of detection and false-alarm rate. The remaining figures show similar plots for four frequencies and two polarizations.

Table 2
Operating Conditions, Sept. 1964 Flights; Antenna Scanning, Transmitted Polarization V, H

Date	Run	Pulse Width (sec)	PRF (pps)	Elev. Angle (degrees)	Azimuth Angle (degrees)	Sample Size
Sept. 8, 64	55	0.25	394	5-1/2	30 L - 90 R	42,800
	56			4-1/2	130 L - 0 R	48,700
	57			4-1/2	60 L - 60 R	33,400
	60			5	180 L - 45 R	19,500
	61			5	60 L - 60 R	32,500
	67			9	150 L - 10 R	24,700
	70			4-1/2	130 L - 20 R	27,700
	71			8	90 L - 60 R	46,500
	103			5-1/2	70 L - 80 R	36,700
	104			4-1/2	70 L - 80 R	40,800
Sept. 12, 64	110	0.25	788	5	70 L - 70 R	57,500
	111			7	70 L - 70 R	107,400
	112			7	70 L - 70 R	46,900
	113			6	70 L - 70 R	81,500
	114			5	70 L - 70 R	66,200
	116			5	70 L - 70 R	82,700
	117			5	70 L - 70 R	83,100
	120			5	70 L - 70 R	41,000
Sept. 13, 64	161	0.5	788	3	70 L - 70 R	61,200
	162			3	70 L - 70 R	71,700
	163			3	70 L - 70 R	37,700
	165			2	70 L - 70 R	46,400
	166			2-1/2	70 L - 70 R	42,700
	167			5	70 L - 70 R	32,400
	170			5	70 L - 70 R	83,300
Sept. 16, 64	64	1.0	394	5-1/2	±50	16,600
	65			7	±50	11,700
	66			6-1/2	110 L - 50 R	35,500
	67			5	110 L - 50 R	26,500
	70			5	110 L - 50 R	26,800
	71			4	110 L - 50 R	17,800
	72			3-1/2	100 L - 40 R	30,700
	73			3-1/2	90 L - 40 R	21,500
	74			3-1/2	90 L - 40 R	41,500

Table 3
Cumulative Distribution of Normalized Cross Section, X Band
Sept. 8, 1964

Run	Polarization	Percentiles					
		90	75	50	25	10	0
55	VV		-40.50	-35.00	-29.25	-24.00	-16.75
	HH				-31.75	-25.00	-17.50
	VH						-24.50
	HV			-40.50	-36.75	-33.00	-24.75
56	VV		-37.50	-32.50	-27.50	-23.00	-16.00
	HH				-31.75	-26.00	-18.50
	VH						-24.25
	HV			-38.50	-36.00	-32.00	-27.00
57	VV			-32.00	-28.50	-24.75	-15.50
	HH						-16.00
	VH	No data					
	HV	No data					
60	VV		-35.00	-30.50	-26.50	-23.25	-15.00
	HH			-32.75	-26.25	-22.50	-15.50
	VH	No data					
	HV	No data					
61	VV		-35.50	-30.50	-25.50	-20.75	-10.00
	HH				-26.50	-22.00	-14.25
	VH	No data					
	HV	No data					
67	VV	-34.50	-29.25	-24.50	-21.00	-18.50	-11.50
	HH	-34.50	-28.75	-24.50	-21.00	-18.50	-11.50
	VH		-38.5	-31.75	-27.25	-24.50	-19.50
	HV	-43.5	-39.5	-35.00	-30.75	-28.00	-21.50
70	VV			-31.00	-27.00	-23.50	-18.75
	HH				-28.00	-21.00	-16.00
	VH						-23.50
	HV				-33.5	-31.5	-25.50
71	VV	-34.00	-29.50	-24.75	-21.50	-19.0	-13.0
	HH	-32.75	-28.00	-24.50	-21.00	-19.0	-11.5
	VH		-37.50	-31.50	-27.00	-24.50	-19.5
	HV	-43.50	-39.75	-35.50	-31.50	-28.50	-21.5
103	VV	-37.00	-32.50	-27.75	-23.50	-20.00	-14.25
	HH		-35.75	-29.00	-24.50	-22.00	-15.00
	VH				-34.25	-27.00	-23.00
	HV			-39.00	-35.50	-32.50	-26.50
104	VV			-31.00	-27.50	-24.50	-18.50
	HH						-21.00
	VH	No data					
	HV	No data					

(Table continues)

Table 3 (cont'd)
Sept. 12, 1964

Run	Polarization	Percentiles					
		90	75	50	25	10	0
110	VV	-29.50	-24.50	-21.50	-17.50	-14.50	- 4.50
	HH	-34.50	-29.75	-26.50	-23.00	-20.50	-11.00
	VH		-36.00	-31.00	-27.50	-25.50	-20.00
	HV	-41.50	-37.00	-31.75	-28.00	-24.50	-20.00
111	VV	-32.00	-27.00	-22.50	-18.50	-15.50	-11.75
	HH			-27.50	-23.00	-20.50	-14.50
	VH				-31.50	-27.50	-20.00
	HV			-33.75	-29.75	-26.50	-20.25
112	VV	-33.00	-27.00	-19.00	-17.00	-14.75	- 8.00
	HH		-32.50	-25.50	-21.50	-19.00	-14.00
	VH				-30.00	-25.50	-19.00
	HV			-33.75	-28.00	-25.00	-15.50
113	VV	-35.00	-29.75	-24.50	-21.50	-17.00	-11.00
	HH		-33.25	-27.00	-23.25	-21.00	-15.00
	VH				-32.50	-28.50	-22.00
	HV			-35.50	-31.25	-27.50	-19.50
114	VV		-30.00	-24.00	-19.50	-14.50	-12.25
	HH			-26.50	-22.00	-19.50	-14.00
	VH				-30.50	-26.75	-20.5
	HV				-34.00	-30.00	-21.00
116	VV		-30.50	-25.00	-20.75	-17.00	-10.00
	HH			-27.25	-22.75	-20.00	-14.00
	VH				-31.75	-27.50	-20.00
	HV				-31.00	-27.00	-20.00
117	VV	-33.50	-29.00	-24.00	-20.00	-16.50	-11.50
	HH		-31.50	-26.00	-22.00	-19.75	-14.00
	VH				-30.00	-26.50	-20.00
	HV			-34.00	-30.00	-26.50	-20.00
120	VV		-30.50	-24.50	-19.50	-16.00	- 5.50
	HH		-33.00	-27.00	-21.75	-19.00	-10.50
	VH				-29.50	-25.25	-19.50
	HV			-34.00	-29.50	-25.25	-17.00
		Sept. 13, 1964					
161	VV		-32.00	-26.00	-22.00	-18.5	-13.0
	HH		-31.25	-26.50	-22.00	-18.0	-10.0
	VH			-33.50	-30.50	-27.25	-20.00
	HV				-32.00	-28.00	-21.75

(Table continues)

Table 3 (cont'd)
Sept. 13, 1964

Run	Polarization	Percentiles					
		90	75	50	25	10	0
162	VV			-28.00	-23.75	-19.50	-13.50
	HH			-29.50	-24.50	-20.75	-11.50
	VH				-31.00	-27.50	-19.50
	HV				-33.50	-30.50	-24.00
163	VV				-28.25	-23.00	-14.00
	HH				-27.50	-22.50	-11.50
	VH					-29.50	-20.00
	HV					-31.50	-23.00
165	VV					-33.00	-21.00
	HH					-32.00	-24.00
	VH						-28.00
	HV						-30.00
166	VV				-21.00	-16.50	- 3.75
	HH				-21.50	-16.75	+ 1.50
	VH						-17.5
	HV						-20.00
167	VV			-29.50	-21.50	-17.00	-13.00
	HH			-31.25	-23.00	-18.00	-11.00
	VH				-29.50	-25.25	-18.00
	HV				-31.50	-27.25	-21.25
170	VV			-29.00	-22.50	-18.50	-13.00
	HH			-29.25	-23.00	-18.50	-11.00
	VH				-30.00	-26.00	-19.00
	HV				-29.50	-25.00	-18.25
Sept. 16, 1964							
64	VV		-30.00	-24.50	-20.50	-18.00	-12.50
	HH		-27.25	-25.75	-23.50	-21.50	-16.00
	VH				-27.50	-25.50	-21.50
	HV				-32.50	-27.50	-22.00
65	VV		-30.00	-24.50	-20.25	-18.10	-12.50
	HH		-27.75	-25.25	-23.00	-21.00	-16.50
	VH				-26.50	-25.00	-21.50
	HV				-31.00	-27.50	-20.00
66	VV		-28.00	-23.00	-19.00	-17.00	-10.00
	HH		-27.00	-24.00	-21.50	-19.50	-13.00
	VH			-28.00	-26.00	-24.25	-19.50
	HV			-34.75	-28.00	-25.00	-18.00

(Table continues)

Table 3 (cont'd)
Sept. 16, 1964

Run	Polarization	Percentiles					
		90	75	50	25	10	0
67	VV		-32.50	-25.50	-21.00	-15.25	-10.00
	HH			-24.50	-22.50	-20.00	- 5.50
	VH					-24.50	-20.00
	HV					-28.00	-20.00
70	VV			-25.50	-21.00	-18.00	-11.50
	HH			-25.00	-22.50	-20 50	-15 00
	VH					-25.00	-20.50
	HV					-29.00	-21.00
71	VV				-27.50	-22.75	-14.50
	HH				-23.50	-21.50	-17.00
	VH						
	HV						-26.50
73	VV				-26.25	-22.50	-15.00
	HH			-24.50	-22.25	-20.50	-16.00
	VH					-23.50	-20.00
	HV						-22.50
74	VV				-29.00	-23.00	-15.00
	HH				-23.00	-21.00	-16.00
	VH					-24.00	-20.50
	HV						-21.75

Table 4
Operating Conditions, July 2, 1965 Flight; Pulse Width 0.5 μsec, PRF 788 pps, Elevation Angle 8 Degrees

Run	Azim. Angle (degrees)	Antenna Scanning	Trans. Pol.	Sample Size
1	60 L-60 R	Yes	V, H	138,000
2	2 R	No	V, H	93,000
3	25 R	No	V	187,000
4	20 R	No	H	40,000
6	60 L-60 R	Yes	V, H	104,000
7	5 L	No	V, H	94,000
10	25 R	No	V	115,000

Table 5
Cumulative Distribution of Normalized Cross Section
July 2, 1965

Run 1

Frequency and Polarization	Percentiles					
	90	75	50	25	10	0
X_{VV}	-33.5	-30	-25.5	-22.5	-20	-14
C_{VV}	-37	-32	-27.5	-24.5	-22	-15.5
L_{VV}	-44.5	-39	-33.5	-30	-26.5	-18.5
P_{VV}	-50.5	-44.5	-39	-35	-32	-22.5
X_{HH}	-34	-30	-25.5	-22	-19.5	-14.5
C_{HH}	-39	-35	-30	-26	-23	-15.5
L_{HH}	-41.5	-38.5	-33	-30	-26	-14
P_{HH}	-43.5	-38.5	-34	-30	-26.5	-14

Run 2

Frequency and Polarization	Percentiles					
	90	75	50	25	10	0
X_{VV}	-34.5	-31	-26	-23.5	-21	-14.5
C_{VV}	-36.5	-31.5	-26.5	-24	-21.5	-15.5
L_{VV}	-42	-36.5	-32.5	-27	-23	-13
P_{VV}	-50.5	-44	-39	-35	-30.5	-21.5
X_{HH}	-33.5	-29.5	-25.5	-22.5	-19.5	-12.5
C_{HH}	-39	-36	-30.5	-27	-24	-17
L_{HH}	-41	-37	-31.5	-27	-22	-9
P_{HH}	-37	-33	-29	-25	-22	-16.5

(Table continues)

Table 5 (cont'd)

Run 3

Frequency and Polarization	Percentiles					
	90	75	50	25	10	0
X_{VV}	-34	-30.5	-25.5	-23	-20	-14
C_{VV}	-37.5	-32	-27.5	-24.5	-21.5	-15.5
L_{VV}	-43	-37.5	-33	-29	-26.5	-18.5
P_{VV}	-	-50.5	-43	-38	-34	-24
X_{HH}						
C_{HH}	H Polarization Not Transmitted					
L_{HH}						
P_{HH}						
X_{VH}	-39.5	-36.5	-33	-29	-26.5	-21
C_{VH}	-	-39	-37.5	-33	-30	-24
L_{VH}	-	-42.5	-41.5	-39.5	-37	-29.5
P_{VH}	-	-	-51	-47	-41	-32.5

Run 4

Frequency and Polarization	Percentiles					
	90	75	50	25	10	0
X_{VV}						
C_{VV}	V Polarization Not Transmitted					
L_{VV}						
P_{VV}						
X_{HH}	-35.5	-31	-27	-24	-21.5	-14
C_{HH}	-39	-37	-31.5	-28	-24.5	-15.5
L_{HH}	-42	-40	-35.5	-31.5	-28.5	-15.5
P_{HH}	-44	-39	-32	-27.5	-24.5	- 7.5
X_{HV}	-42	-38	-34	-31.5	-29	-22.5
C_{HV}	-44	-41.5	-37	-33.5	-30.5	-23
L_{HV}	-48.5	-46	-42.5	-38.5	-35.5	-26.5
P_{HV}	-	-	-51	-26.5	-43	-32

(Table continues)

Table 5 (cont'd)

Run 6

Frequency and Polarization	Percentiles					
	90	75	50	25	10	0
X_{VV}	-34.5	-31	-26	-23	-20	-11.5
C_{VV}	-37	-31.5	-27	-24	-20.5	-10
L_{VV}	-41	-36.5	-32.5	-27.5	-24.5	-15
P_{VV}	-44	-39.5	-34.5	-30	-27	-21
X_{HH}	-33.5	-29	-24.5	-21	-16.5	- 3.5
C_{HH}	-38.5	-34.5	-27.5	-23	-18.5	- 3.5
L_{HH}	-42	-38.5	-34	-29.5	-25.5	-12.5
P_{HH}	-47	-41	-36	-32	-27.5	-18.5

Run 7

Frequency and Polarization	Percentiles					
	90	75	50	25	10	0
X_{VV}	-36	-32	-28.5	-25	-22	-14.5
C_{VV}	-37	-32.5	-28	-24.5	-22	-15.5
L_{VV}	-40.5	-36	-32	-27.5	-26	-18.5
P_{VV}	-45.5	-41.5	-37.5	-34	-31.5	-23
X_{HH}	-35	-31	-27	-24	-21.5	-15.5
C_{HH}	-39	-36.5	-30	-27	-24	-17
L_{HH}	-41.5	-37	-33	-28.5	-26	-18.5
P_{HH}	-42	-38	-34	-31	-28	-22.5

(Table continues)

Table 5 (cont'd)

Run 10

Frequency and Polarization	Percentiles					
	90	75	50	25	10	0
X_{VV}	-38	-34	-29	-25	-22.5	-16.5
C_{VV}	-41	-35.5	-30.5	-25.5	-23.5	-17
L_{VV}	-40.5	-36.5	-32.5	-27.5	-26	-18.5
P_{VV}	-44.5	-39	-34.5	-30.5	-26.5	-21
X_{HH}						
C_{HH}	H Polarization Not Transmitted					
L_{HH}						
P_{HH}						
X_{VH}	-40	-38.5	-35	-30.5	-27.5	-21
C_{VH}	-	-39	-38	-33.5	-30	-23 5
L_{VH}	-42.5	-42	-40.5	-36.5	-34	-25
P_{VH}	-	-53	-47.5	-42	-39	-32.5

Table 6
Operating Conditions, Dec. 10, 1964 Flight

Run	Pulsewidth (μsec)	PRF (pps)	Elev. Angle (degrees)	Azim. Angle (degrees)	Antenna Scanning	Trans. Pol.	Sample Size
57	0.25	1576	4	20		V, H	33,096

Using the July 1965 data, the wavelength dependence of the terrain clutter was determined. Two presentations of the dependence are demonstrated; the first, Fig. 12a, has the range of values of the normalized clutter cross section as a function of the wavelength. Figure 12b gives the ratio of the clutter cross sections as a function of the wavelength ratio. Six such ratios may be obtained, and the range of values is shown. The solid line in each figure is the locus of values which would be obtained for an inverse first power of the wavelength dependence. The data used for these graphs are the median values of clutter cross section obtained from the runs taken on this day. The polarization was chosen to be vertical transmit and receive, although horizontal

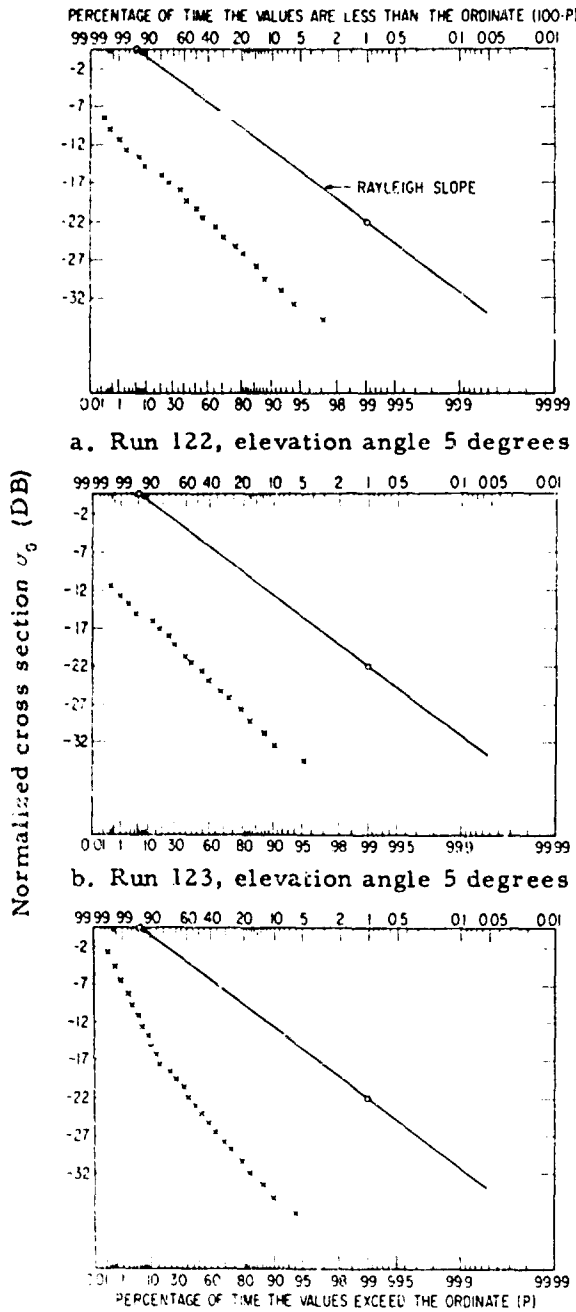

a. Run 122, elevation angle 5 degrees

b. Run 123, elevation angle 5 degrees

c. Run 125, elevation angle 6 degrees

Fig. 9 - Measured clutter distributions compared with assumed distributions (Rayleigh slope); Sept. 12, 1964, VV polarization, X band

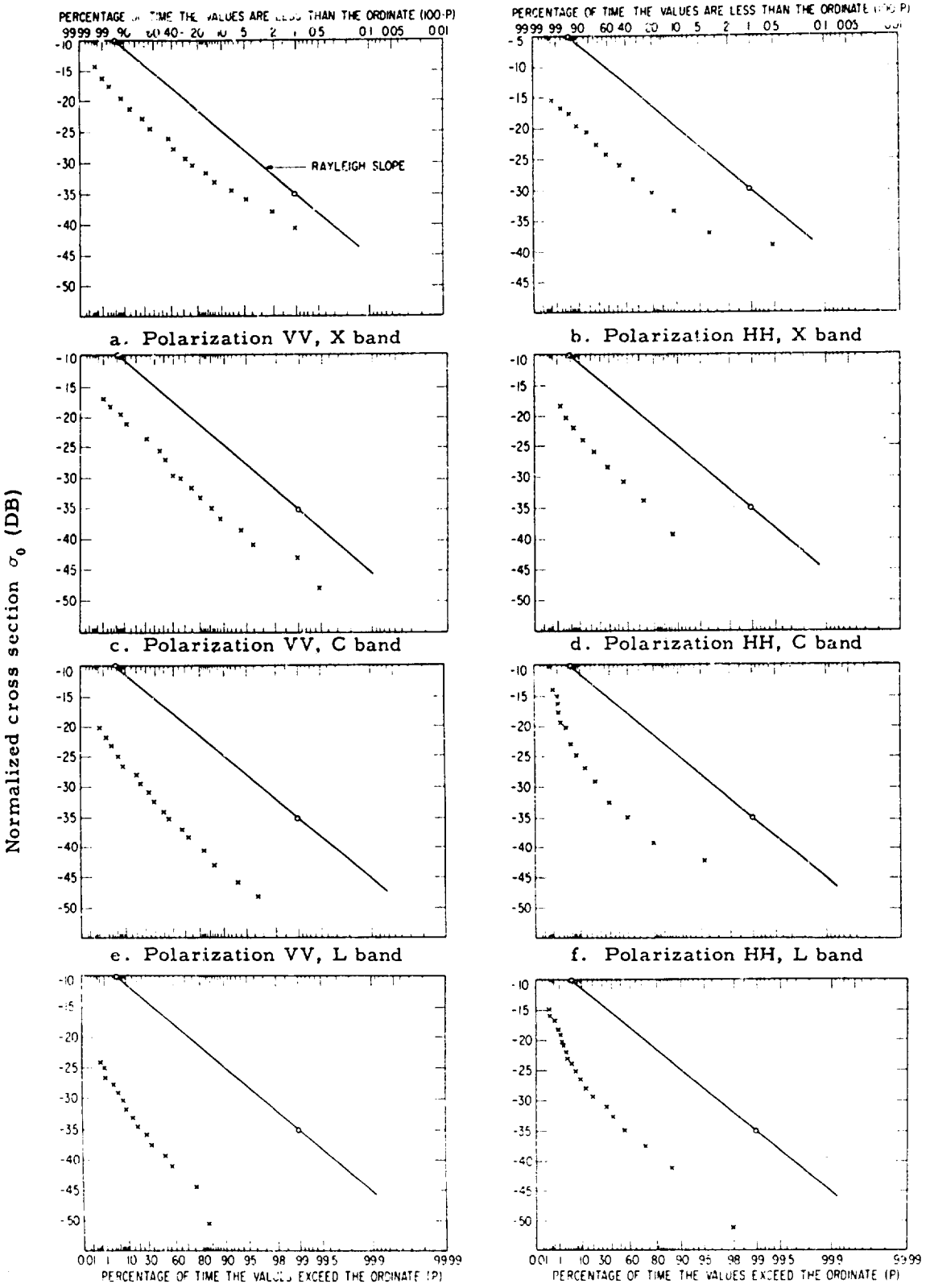

Fig. 10 - Measured clutter distributions compared with assumed distributions (Rayleigh slope); July 2, 1965, run 1

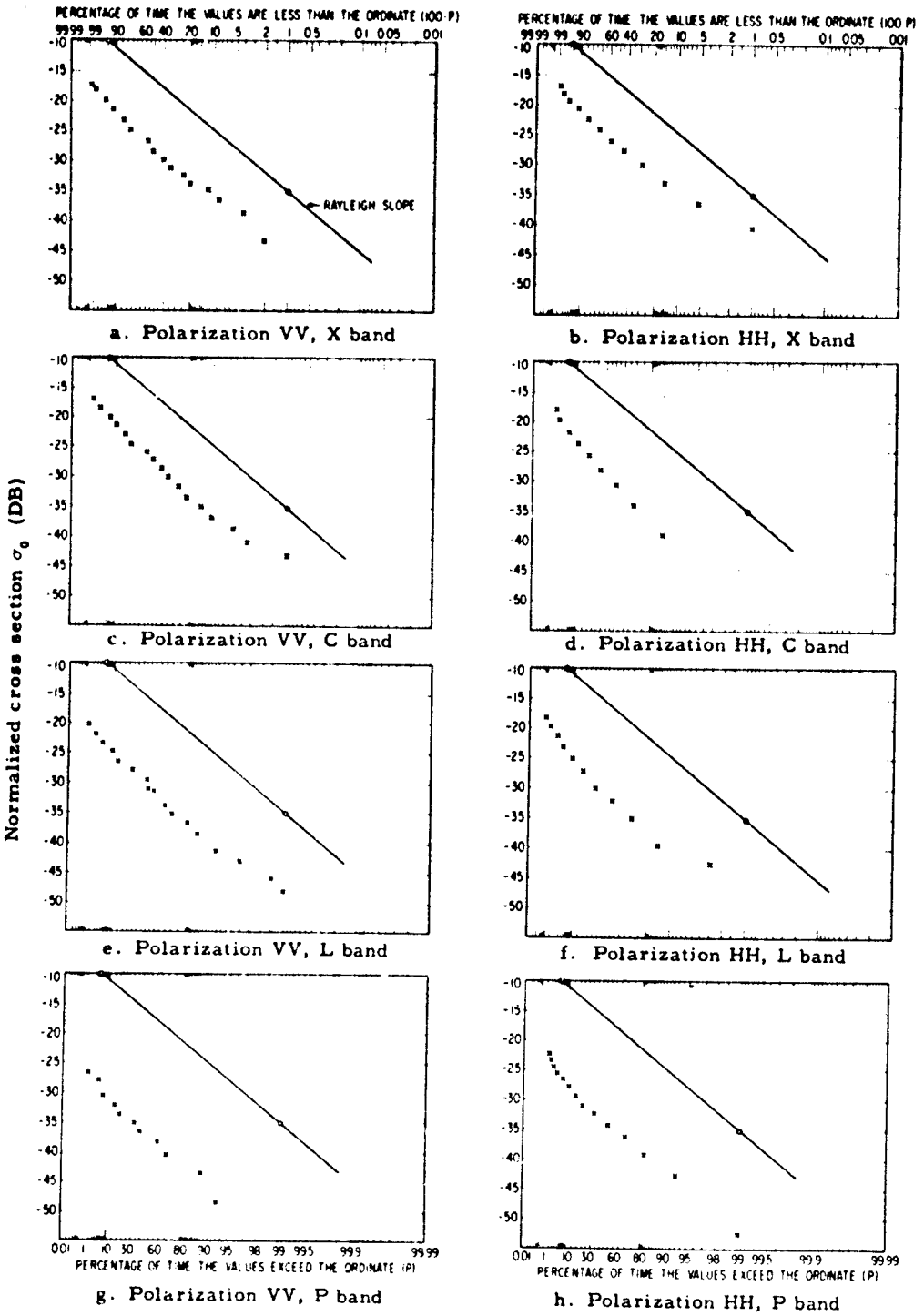

a. Polarization VV, X band

b. Polarization HH, X band

c. Polarization VV, C band

d. Polarization HH, C band

e. Polarization VV, L band

f. Polarization HH, L band

g. Polarization VV, P band

h. Polarization HH, P band

Fig. 11 - Measured clutter distributions compared with assumed distributions (Rayleigh slope); July 2, 1965, run 7

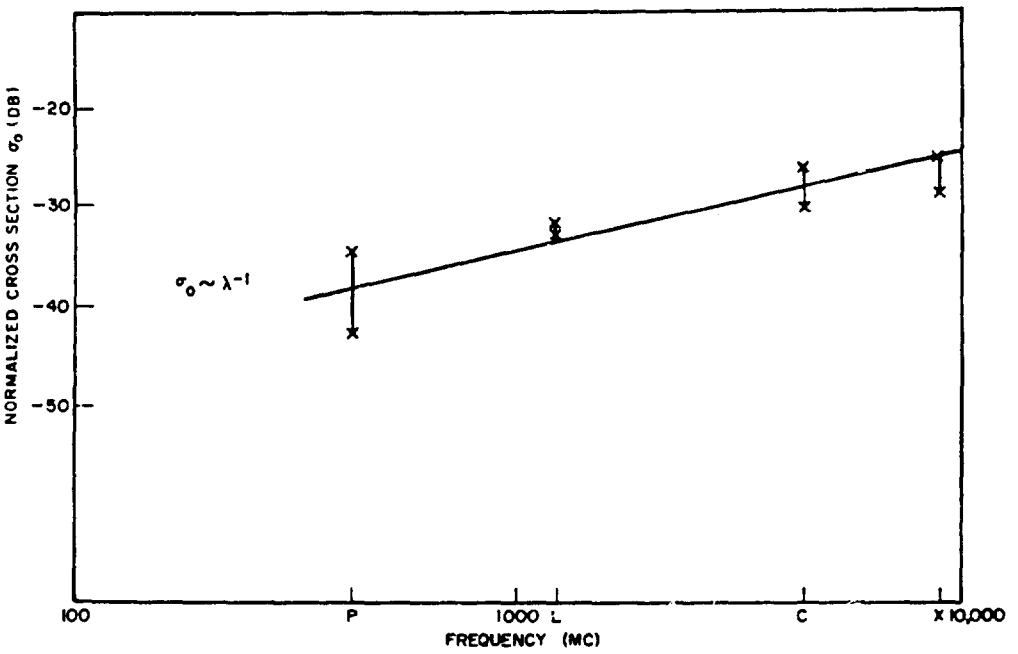

a. Normalized clutter cross section as a function of wavelength

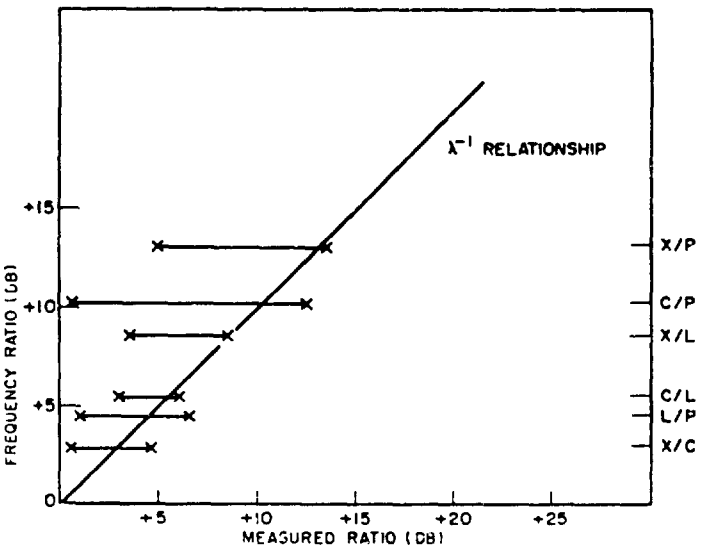

b. Ratio of clutter cross sections as a function of wavelength ratio

Fig. 12 - Wavelength dependence of terrain clutter

transmit and receive show little difference in dependence from vertical. This result is consistent both with previous NRL measurements and also those taken in this wavelength range by Ohio State University. Much of the previous data are presented by L. Katz of Applied Physics Laboratory of Johns Hopkins University in a paper entitled "Wavelength Dependence of the Radar Reflectivity of Earth and Moon," Vol 71, No. 2, Journal of Geophysical Research, Jan 15, 1966. Katz has shown that the radar cross section on the average is a decreasing function of wavelength to approximately the first power,

with exceptions whose dependence varies from +2nd to -6th power of the wavelength. The positive values of the exponent are found in the dependence of snow-covered surfaces at all depression angles and of the sea surface above 73 degrees of depression.

It is well known that the clutter cross section is strongly influenced by the terrain. Two types of variations may be defined: the relatively rapid fluctuations produced by the change in phase of the scattered energy produced by internal or aircraft motion, and the relatively slow variation produced by gradual changing of the terrain character. These slow variations constrain the sample time over which a distribution may be considered stationary. An example of both such fluctuations is shown in Fig. 13. This run was taken over Pisgah Crater, California. In order to specify the nature of the scattering terrain, photographic imagery was used both down looking and along the bore site of the antenna. This picture was combined with USGS aerial survey maps of the area to produce a flight path superimposed on the terrain synchronized with the time track of the recorded data. The data show graphically the need for including both the fast fluctuations and slow fluctuations of the clutter signals in any model which is to be representative of the terrain-clutter return.

Clutter Spectra

The apparent velocity of the clutter patch illuminated by the radar is given by:

$$v = v_a \cos \psi_0 \cos (\psi_0 + \Delta\psi) \tag{10}$$

where v_a is the aircraft velocity; ψ_0 and ψ_0 are the elevation and azimuth angles of the beam center, and $\Delta\psi$ is the angular position of scatterers in the patch with respect to beam center. For pulsed radars, the variation in elevation angle over the patch may be neglected. The motion of the patch produces a Doppler shift, f, in the carrier given by:

$$\Delta f = 2v_g / \lambda \cos (\psi_0 + \Delta\psi) \tag{11}$$

where v_g is the ground speed of the aircraft, and λ the transmitted wavelength. The variation in the Doppler shift across the patch gives rise to a spectrum centered at:

$$f_0 = \frac{2v_g}{\lambda} \cos \psi_0 \tag{12}$$

whose width is a function of $\Delta\psi$. For a nominal ground speed of 300 ft/sec, the spectrum centered at X band has a maximum value of 5454 cps, while at C, L, and P bands, the center is located at 2727 cps, 909 cps, and 248 cps respectively. The maximum prf's available in the 4F radar system are 1576 pps (single polarization) or 1463 pps (alternating polarization). If the radar pulse is considered as sampling the Doppler return, then ambiguity results, since the sampling rate is less than the spectrum center frequency. Doppler or velocity ambiguity is a possibility in three of the four frequencies. The P-band spectrum is unambiguous. As a result of the ambiguity in X, C, and L (at forward angles), spectra will exist at centers, f_n, given by:

$$f_n = f_0 + nf_r \tag{13}$$

where f_r is the pulse-repetition frequency. Assuming a value of 5454 cps for the X-band Doppler center and f_r equal to 1576 pps, representative X-band Doppler spectra will be centered at 726 cps, 850 cps, 2302 cps, and at infinitely many other locations. It is characteristic of the sampling process that the maximum energy is located in the spectrum centered between zero and one-half prf. It is also characteristic that only one spectrum will exist in this range. The spectrum centered at 726 cps differs from the sampled spectrum in two respects: a constant amplitude factor and a constant frequency shift. Since

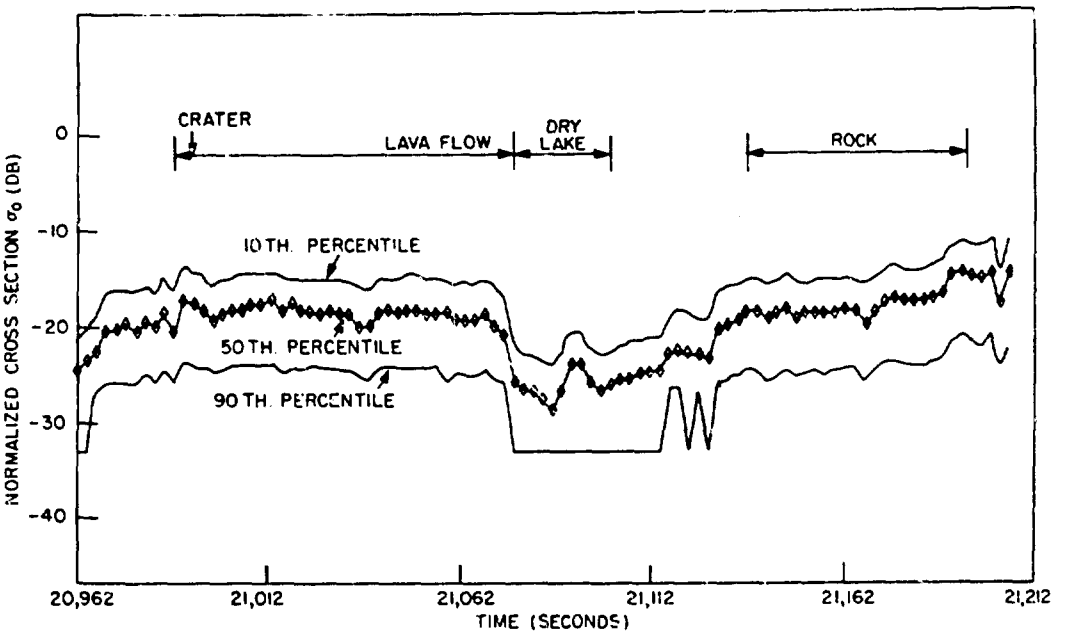

Fig. 13 - Pisgah Crater terrain cross section, Sept 13, 1964, run 14, elevation angle 30 degrees, polarization VV, X band

absolute values of the spectral amplitudes must be determined by calibration, the constant-amplitude factor will be absorbed in the process, while the original frequency axis can be reconstructed from a knowledge of the aircraft velocity and geometry, so that neither of the above-mentioned characteristics is a severe liability. The spectrum centered at 726 cps is termed an "alias" of the original spectrum, since only the frequency label of the spectrum has changed and not the relative shape. The spectra presented in this report, since they involve C-, X-, and L-band transmitted frequencies, are the aliases of the original spectra. The P-band spectra are unique.

If the width of the spectra is such that portions extend beyond the limits, 1/2 prf or prf, a further imaging of the spectra will result, and an alias of the energy above one-half prf will appear at an equal frequency below prf. This phenomenon is termed "foldover" and destroys the usefulness of the spectrum. To avoid foldover, the alias must be positioned roughly midway between zero and one-half prf, since foldover also occurs at zero frequency. The positioning of the spectrum is achieved in the field by the adjustment of ψ_0, the antenna azimuth, which varies the apparent velocity of the clutter patch and thus the frequency of its Doppler alias. It has been possible with X and C bands to find an optimum azimuth so that foldover was avoided on both frequencies. The addition of L band poses a more difficult task, since foldover must be avoided on three separate Doppler aliases simultaneously.

Since the spectrum position is a function of the position angles of the antenna beam and the aircraft velocity, movements of the antenna or changes in velocity will displace the spectra along the frequency axis. Averages of the spectra are necessary, so that considerable editing of the data is required to find portions of the flight path where the variations of the aircraft speed and antenna motion are a minimum. The criterion presently used is that a long time average of the spectra must converge in shape to the antenna pattern as shown in Appendix C. This criterion eliminates much data; however, that which remains is susceptible to statistical analysis.

Two forms of presentation of spectra are shown in this report. The data taken over the Eastern Shore, Maryland are displayed with a linear ordinate, while that shown for Denver, Colorado are displayed with a logarithmic ordinate. The purposes of these presentations differ. The Eastern Shore data shown in Figs. 14 through 17 are a series of spectra which were taken to evaluate the effect of terrain on the antenna spectrum.* If the antenna is subdivided into smaller beams of width $\Delta\psi_a$, then the illuminated area, Eq. (8), is subdivided into patches of width $R\Delta\psi_a$, where R is the range to the patch and length $C\tau/2$. Equation (11) defines a doppler spread of width Δf_a over the smaller area, where the total of all such frequency bands is the total main beam spectrum. The power incident on the clutter patch is given by $P_T G^2(\theta_a, \psi_a)$, where θ_a is the elevation and ψ_a the azimuth of the center of the patch. If the patch has a normalized cross section, σ_{0a}, then the power in the clutter spectrum is

$$P_s = P_T \sum_{a=0}^{A} \sigma_{0a} G^2(\theta_a, \psi_a) \Delta f_a \quad . \tag{14}$$

Since the factors G and Δf_a are time invariant, the power variations along the path are related to the values of S_a, the reflectivity of "ribbons" of terrain of width $R\Delta\theta_a$ parallel to the flight path. In order to determine the distribution of the S_a the phase-versus-time data were analyzed by digital Fourier analysis, which is described in Appendix C, and the standard deviation of the spectral estimates computed. These are shown in Figs. 18 through 21. The solid curve in each figure is the value of $G^2(\theta, \psi)$, the two-way power pattern of the antenna in normalized units. The bars are twice the standard deviation of the spectral estimates in length.

The spectra and the composite spectra document the existence of two radically different types of distribution existing in the terrain ribbons. The first is a random distribution whose 2σ value is approximately equal to the mean, a characteristic possessed by the Rayleigh distribution. The second is a distribution which from inspection of the spectra is produced by strong, sustained signals present in the clutter and may be termed a "signal plus noise distribution" in the sense of Rice (6).

To proceed further, the noncoherent envelope correlation function is defined (7) as

$$Z^2(\tau) = \left[\int_{-\infty}^{\infty} W_c(f') \cos 2\pi f_0 \tau \, df \right]^2 + \left[\int_{-\infty}^{\infty} W_c(f') \sin 2\pi f_0 \tau \, df \right]^2 = \mu_{13}^2 + \mu_{14}^2 \tag{15}$$

where W_c is given in Eq. (1), f_0 is the spectrum center, and τ the tag time. The normalized, but not dc suppressed, incoherent video correlation function is given by

$$\Phi_c(\tau) = \frac{1 + Z^2(\tau)}{2} \tag{16}$$

*Frequency in these and all subsequent figures is measured in cycles per second.

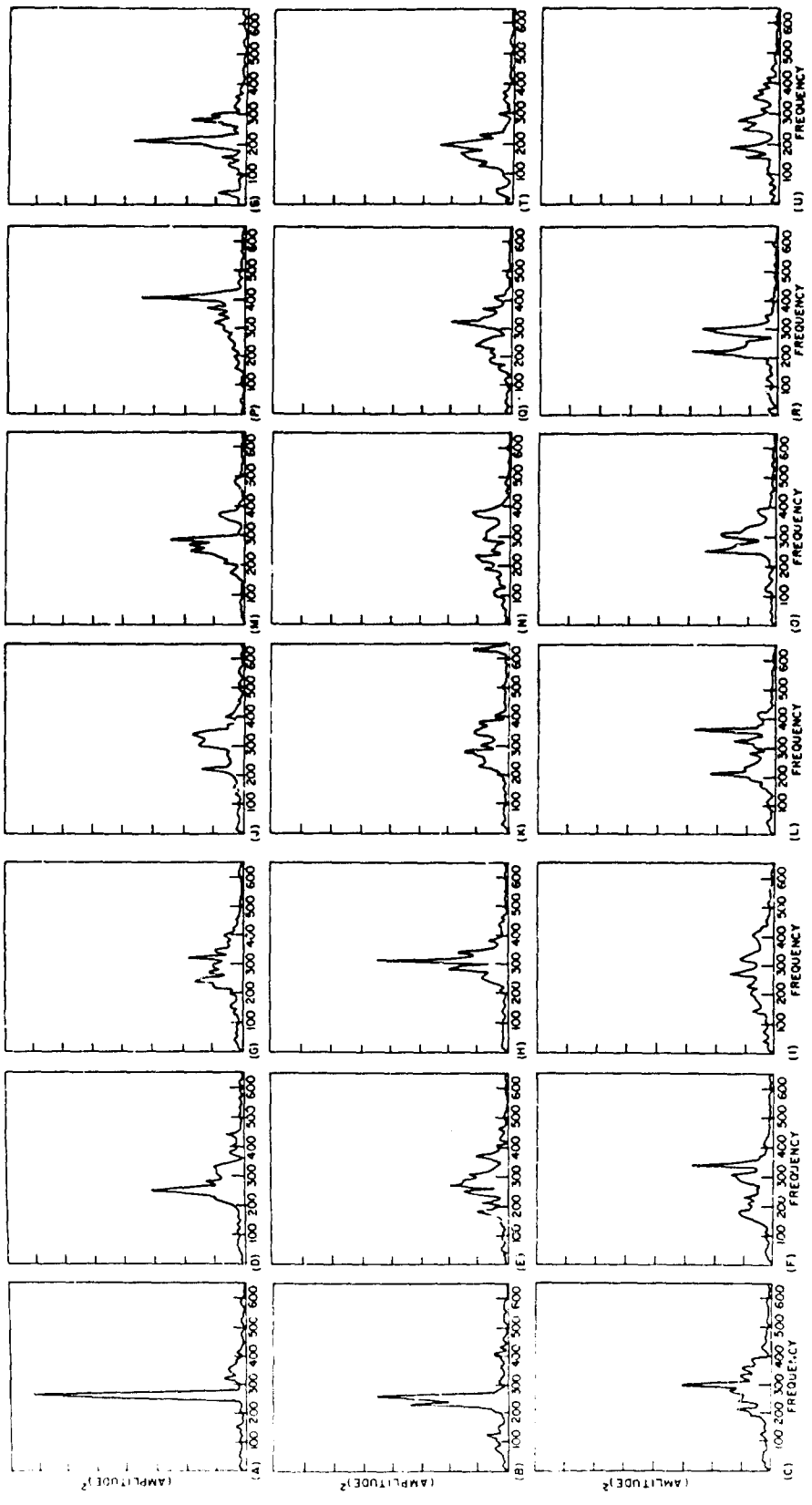

Fig. 14 - Clutter power spectra, Eastern Shore, Md., run 57, elevation angle 4 degrees, X_{HH} return

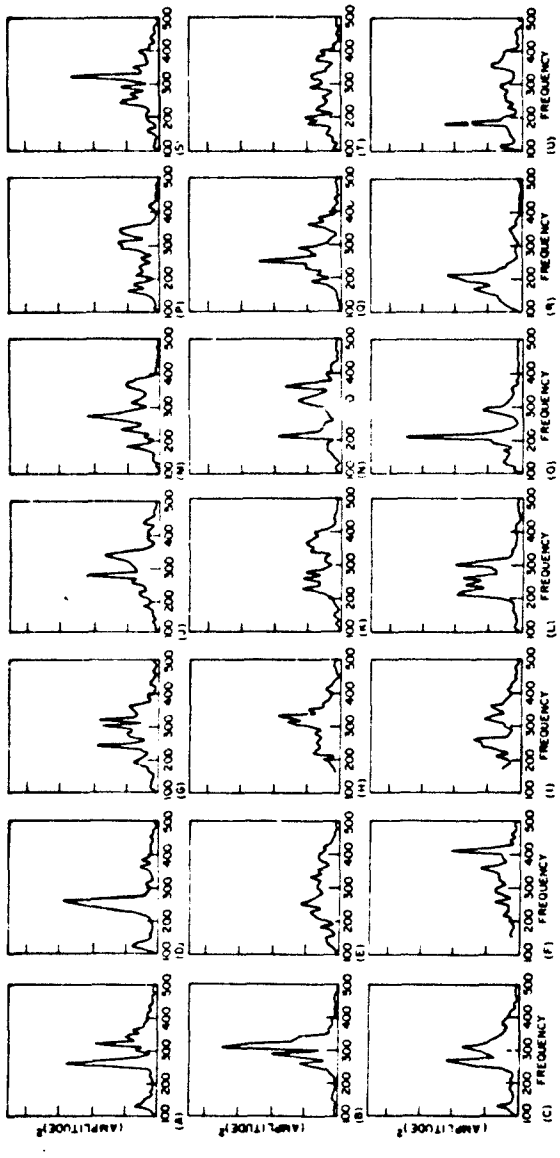

Fig. 15 - Clutter power spectra, Eastern Shore, Md., run 57, elevation angle 4 degrees, X_{VV} return

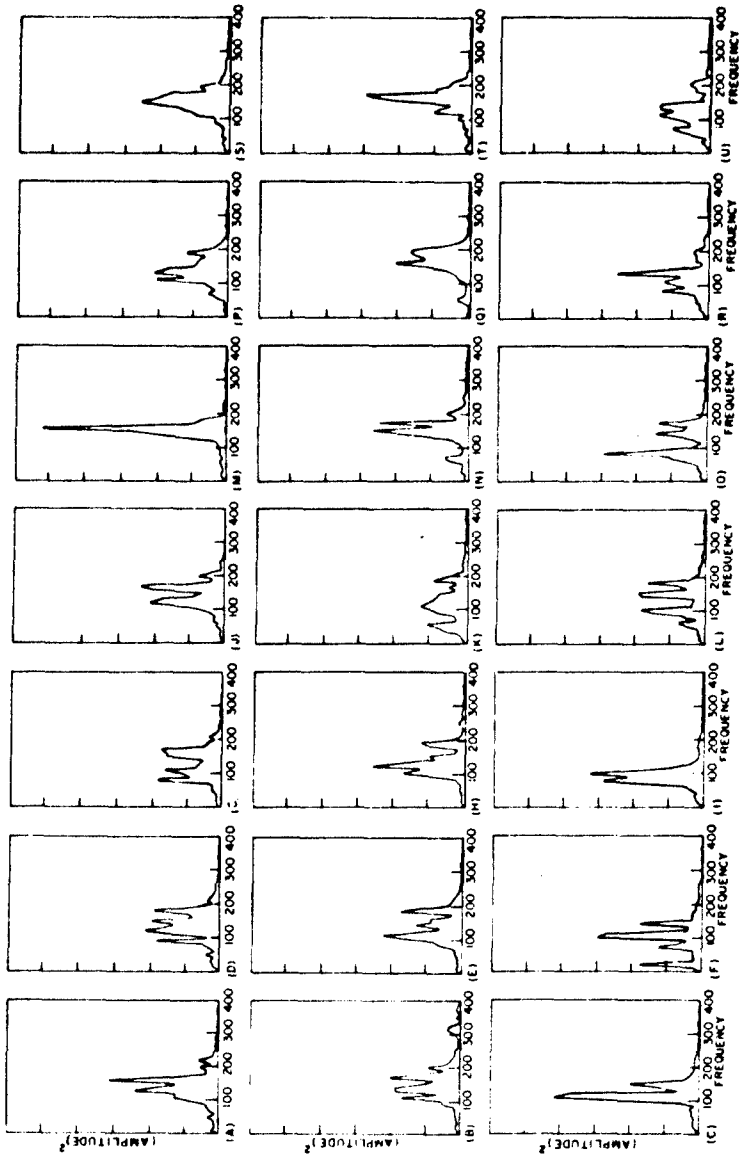

Fig. 16 - Clutter power spectra, Eastern Shore, Md., run 57 elevation angle 4 degrees, C_{VV} return

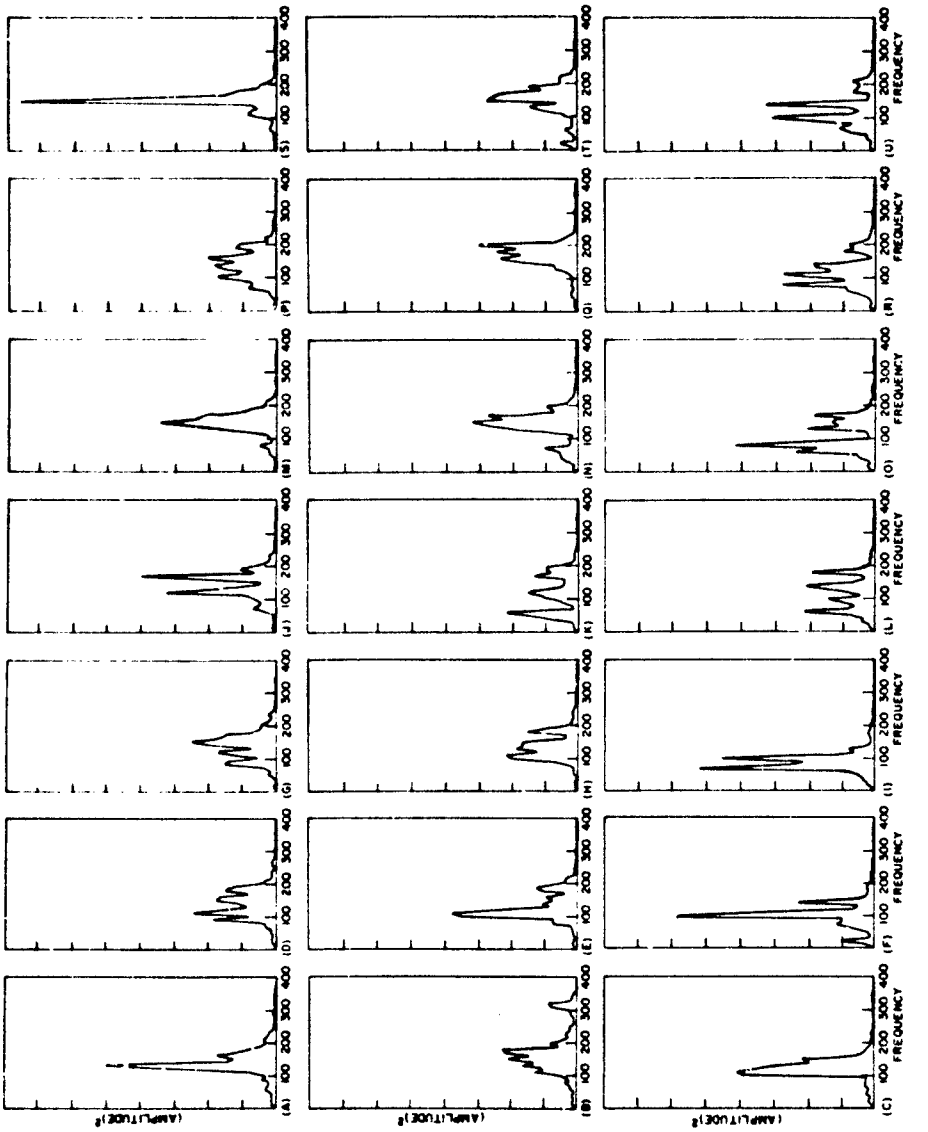

Fig. 17 - Clutter power spectra, Eastern Shore, Md., run 57, elevation angle 4 degrees, C_{HH} return

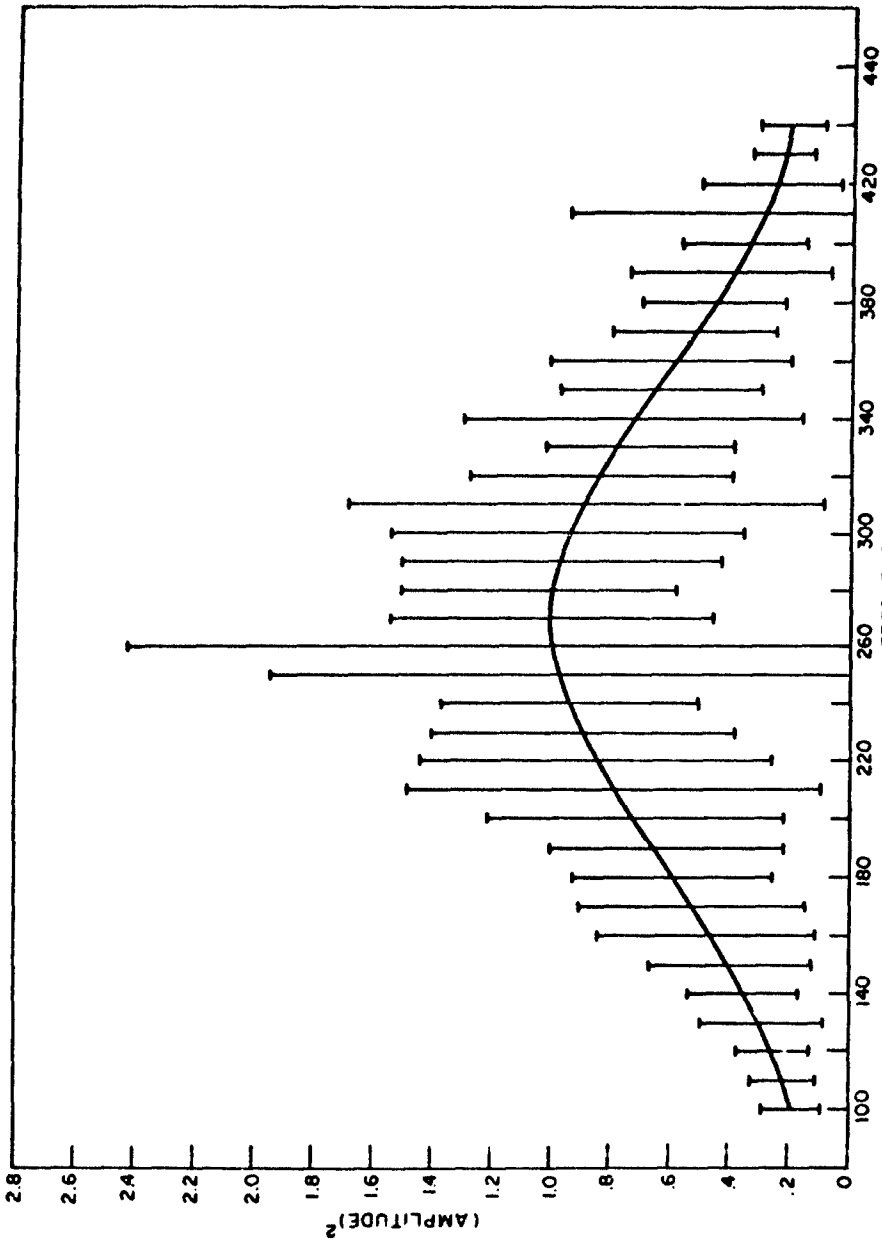

Fig. 18 - Standard deviation of spectrum estimates, run 57, Dec. 10, 1964, time 19013, Eastern Shore, Md., X band, HH polarization, 10 degrees of freedom, 10 cps bandwidth

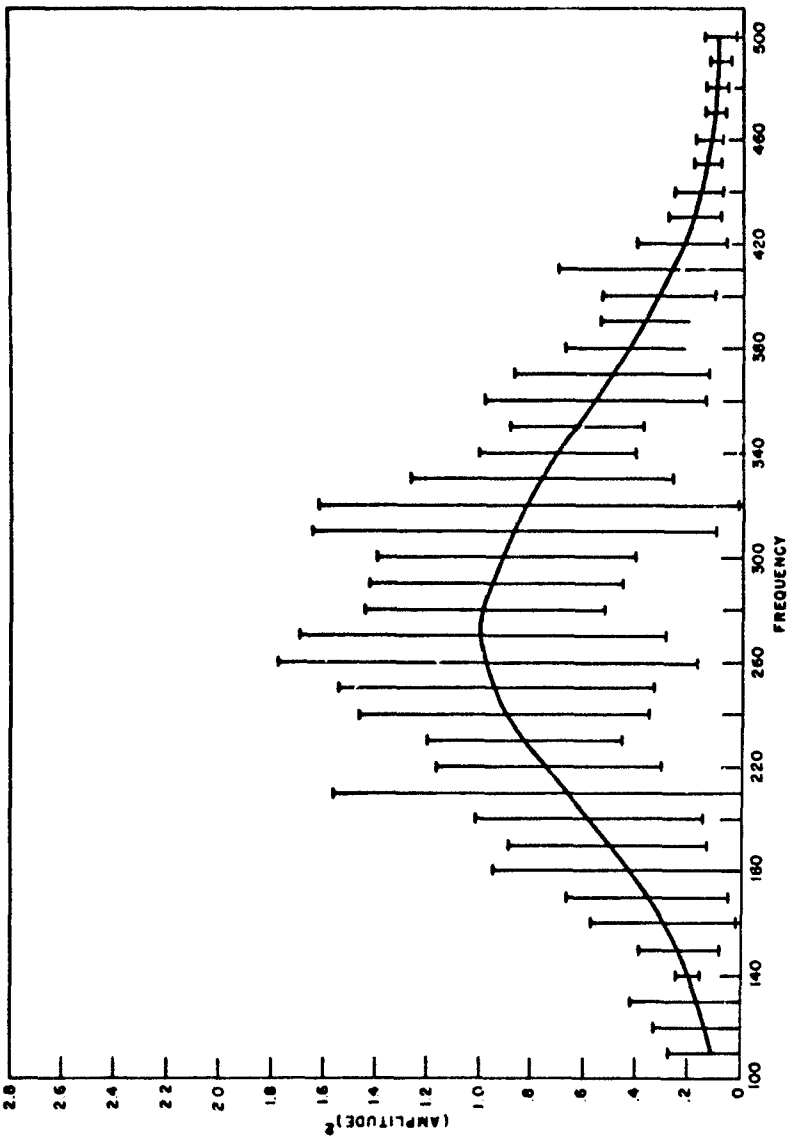

Fig. 19 - Standard deviation of spectrum estimates, run 57, Dec. 10, 1964, time 19013, Eastern Shore, Md., X band, VV polarization, 10 degrees of freedom, 10 cps bandwidth

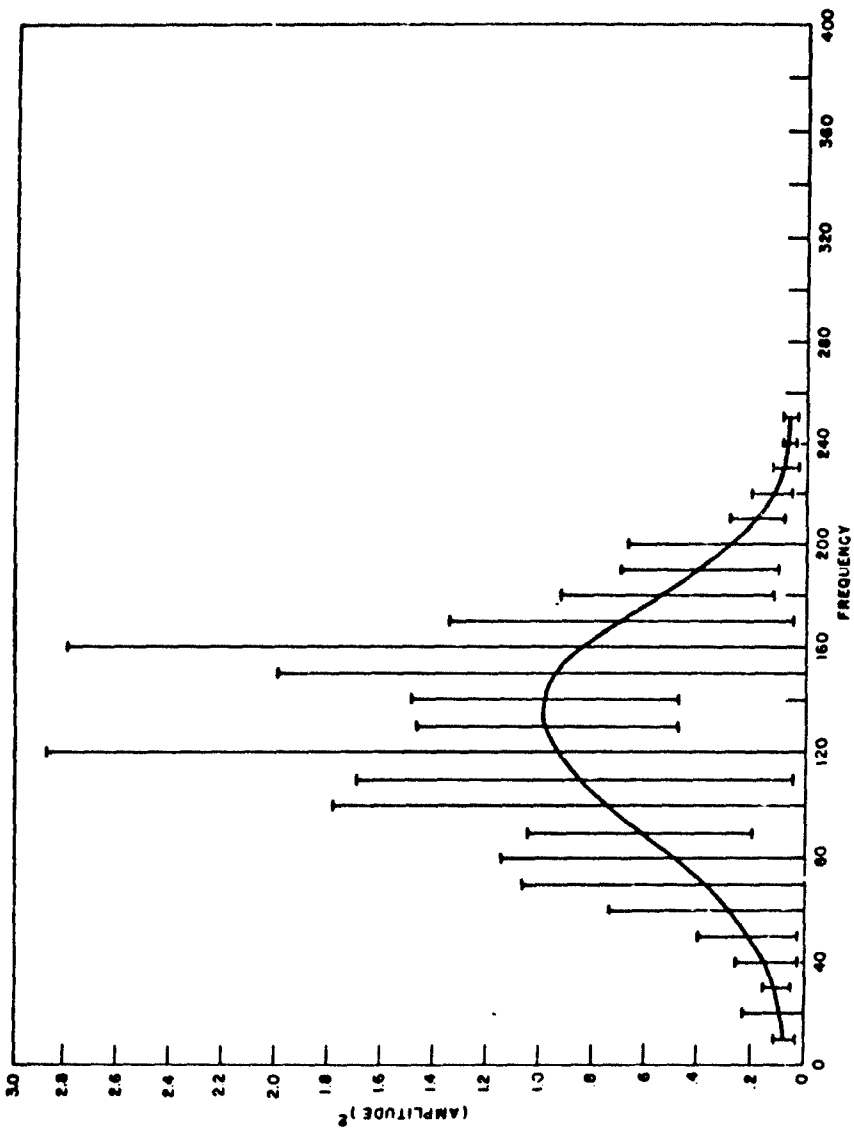

Fig. 20 - Standard deviation of spectrum estimates, run 57, Dec. 10, 1964, time 19013, Eastern Shore, Md., C band, HH polarization, 10 degrees of freedom, 5 cps bandwidth

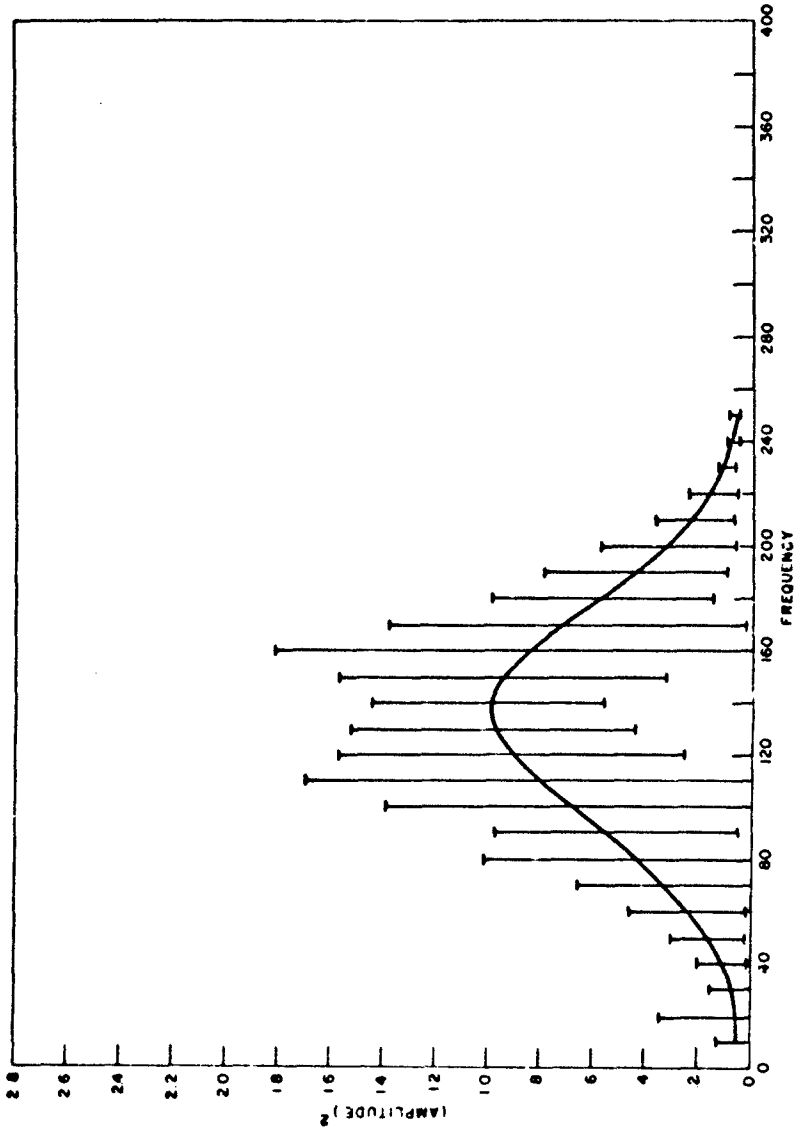

Fig. 21 - Standard deviation of spectrum estimates, run 57, Dec. 10, 1964, time 1901Z, Eastern Shore, Md., C band, VV polarization, 10 degrees of freedom, 5 cps bandwidth

while the pulse-to-pulse phase shift is given by

$$\psi_0(\tau) = \tan^{-1} \frac{\mu_{14}}{\mu_{13}}. \tag{17}$$

The pulse-to-pulse phase shift, , , produced by a point target in the clutter patch, is given by a similar expression, where the spectrum of the target is inserted in Eq. (15). Urkowitz (8) has shown that the combined video correlation function of a fixed point target of amplitude P in a clutter patch whose average power is V^2 is

$$\phi_s(\tau) = \frac{(x+1)^2 + 2x\cos(\psi_0 - \gamma) + Z^2(\tau)}{(x+1)^2 + 2x + 1} \tag{18}$$

where $x = P^2/2V^2$.

The above expression indicates that the pulse-to-pulse noncoherent correlation function is strongly affected both by the amplitude and position of the strong point scatterer. The coherent correlation function, which is proportional to the square root of the incoherent function, is similarly affected. Since, as will be noted in the next section, clutter-cancellation techniques use the pulse-to-pulse correlation to reject clutter, the knowledge of both the Rayleigh-distributed clutter patches and the signal-plus-noise-distributed patches is extremely important to the prediction of radar performance in clutter.

The spectra shown in Figs. 22 through 29 are spectra taken on the Denver trip, July 1965. The logarithmic axes used to present these spectra preserve the maximum dynamic range available in the quantized output of the phase detector. The major interest in these spectra is their uniqueness, in that in conjunction with the cumulative distributions given in Table 5 for this run, they present a nearly complete statistical description of the clutter process over this terrain as a function of wavelength and polarization. In addition, the correlation function which may be derived from these spectra enables the cancellation ratio to be determined over a wide variety of circumstances.

In order to assist other analysts in the use of this data, a brief description of the clutter power spectra presented in this section is included here. This description in conjunction with Appendixes A and C should yield sufficient information to allow general use of the information. Table 6 gives the operating conditions for the Eastern Shore flight. In the spectra shown in Figs. 14 through 17 an analysis window width of 5 cps was chosen. This value was established by using a sample length of 0.1 sec. This value of window width was chosen primarily to allow rapid processing of the data. Specification of the resolution in a more exact manner requires a knowledge of the spatial dependence of the terrain features which at present is absent, since imagery of the terrain is not available. Both X- and C-band returns were analyzed using the same width. Estimates of the spectra were made at every 10 cps, in X band from 100 to 500 cps, and in C band from 10 to 250 cps. A record of 21 seconds length was available over which the antenna position was relatively stable. This time was determined by the test mentioned previously. It was decided to eliminate the rapid fluctuations produced by the changing phase of the scatterers, to average over ten consecutive spectra of 0.1-sec duration to form the resulting curves. This method also has the advantage of making each spectrum the average over the illuminated area of the beam, since the aircraft travels a distance approximately equal to (2 (0.25-. sec pulse) in one second. Due to a defect in the computer input program, a gap of approximately one third of a second exists between each graph plotted. The spectra

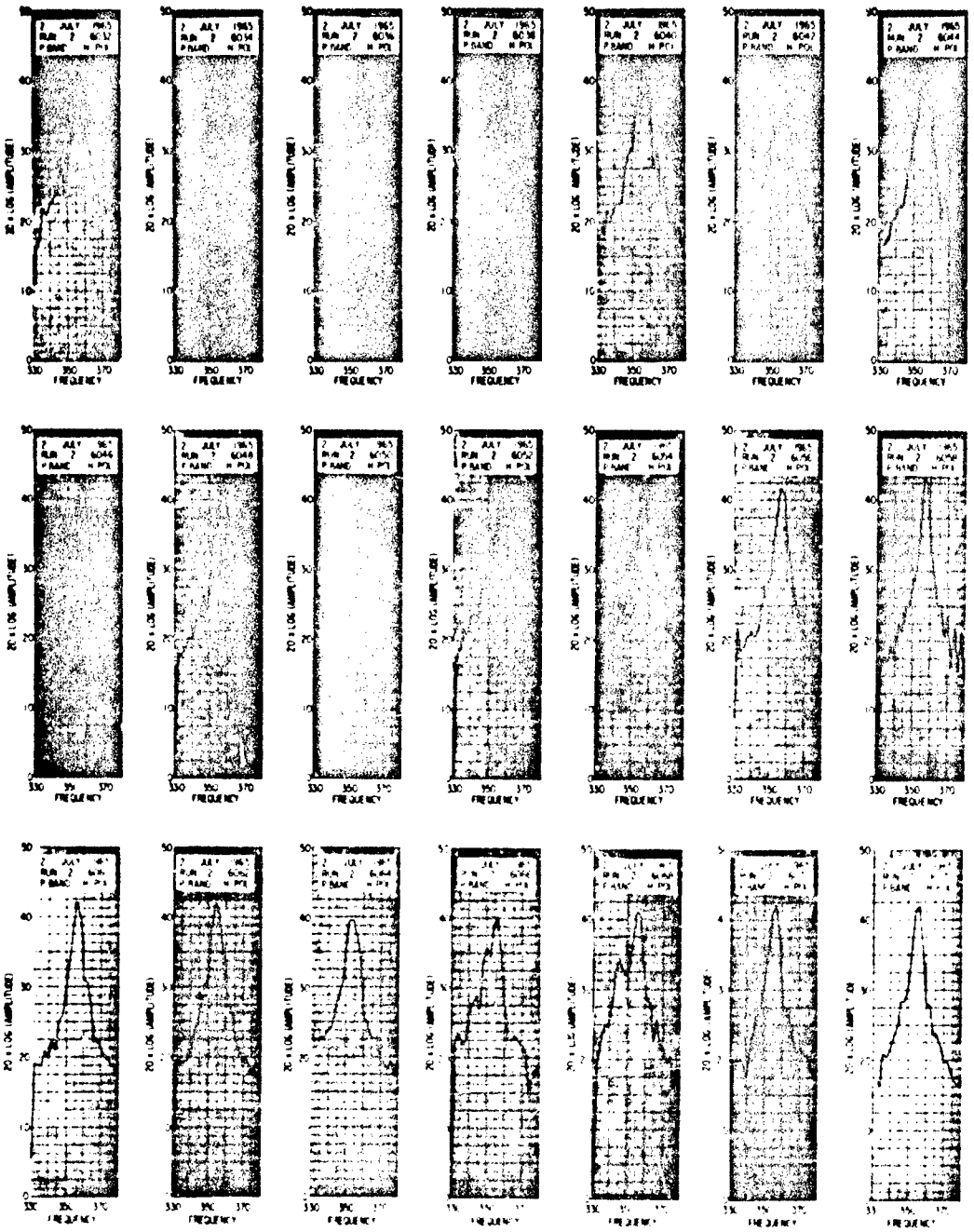

Fig. 22 - Clutter power spectra, July 2, 1965, run 2, P band, HH polarization

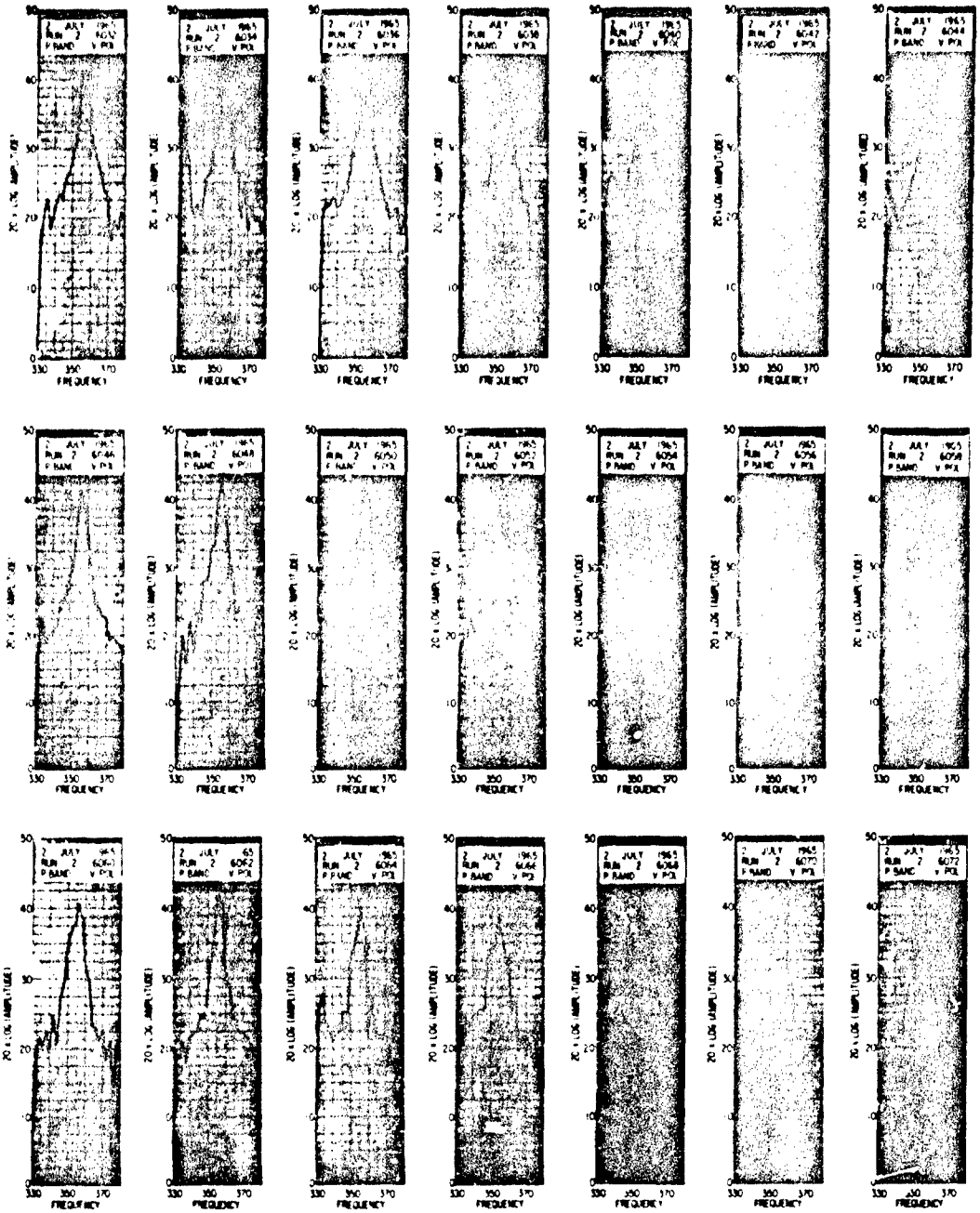

Fig. 23 - Clutter power spectra, July 2, 1965, run 2.
P band, VV polarization

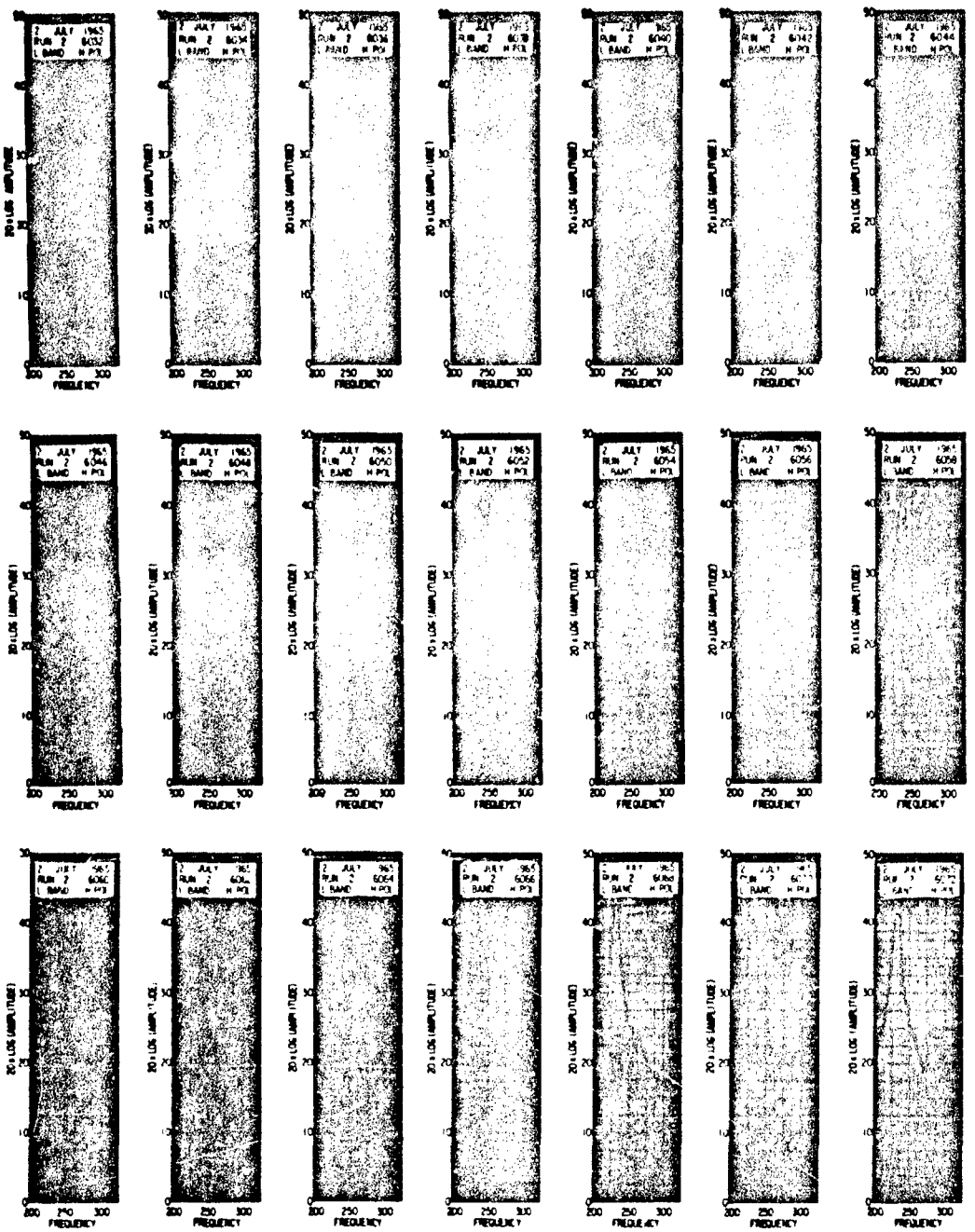

Fig. 24 - Clutter power spectra, July 2, 1965, run 2, L band, HH polarization

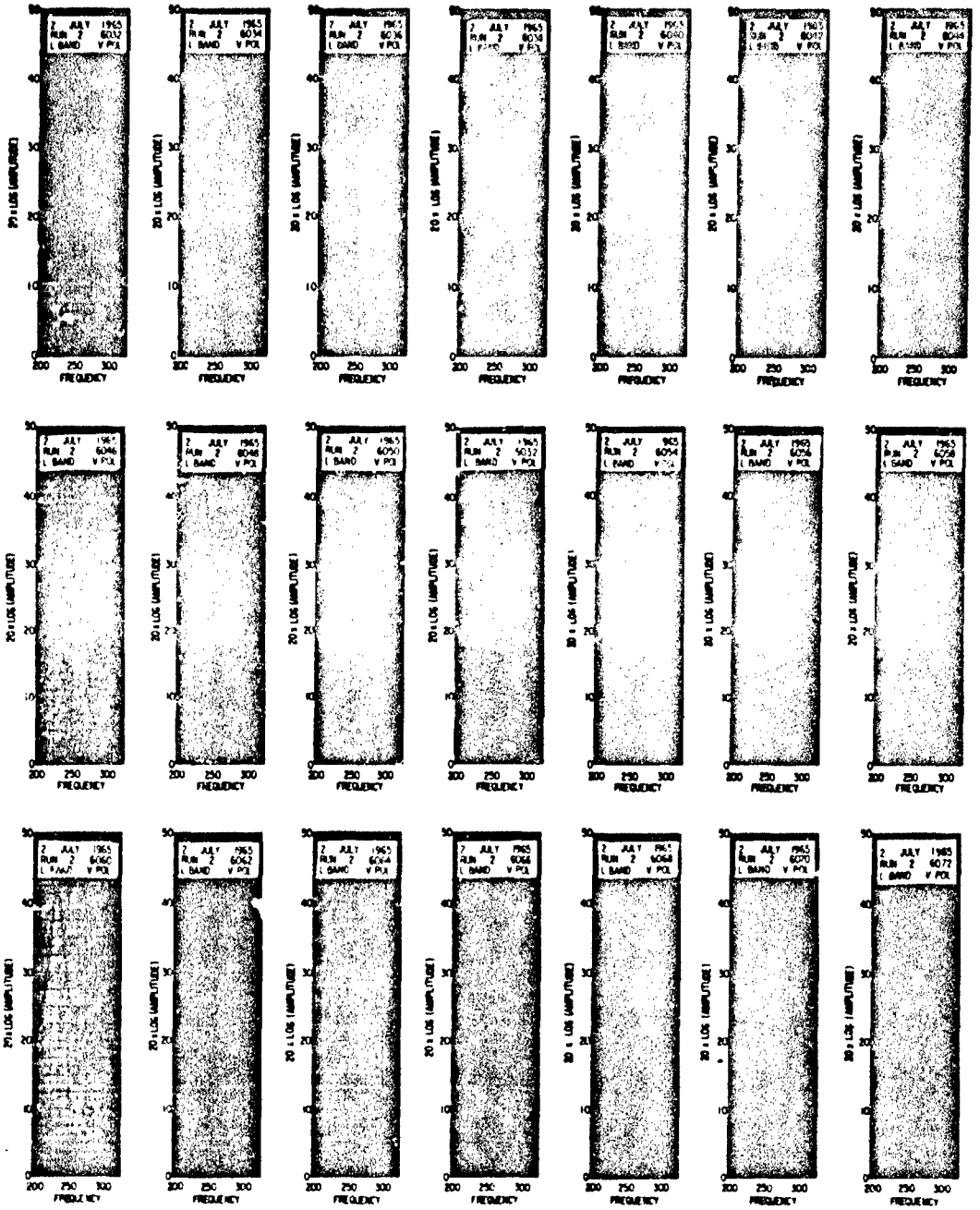

Fig. 25 - Clutter power spectra, July 2, 1965, run 2.
L band, VV polarization

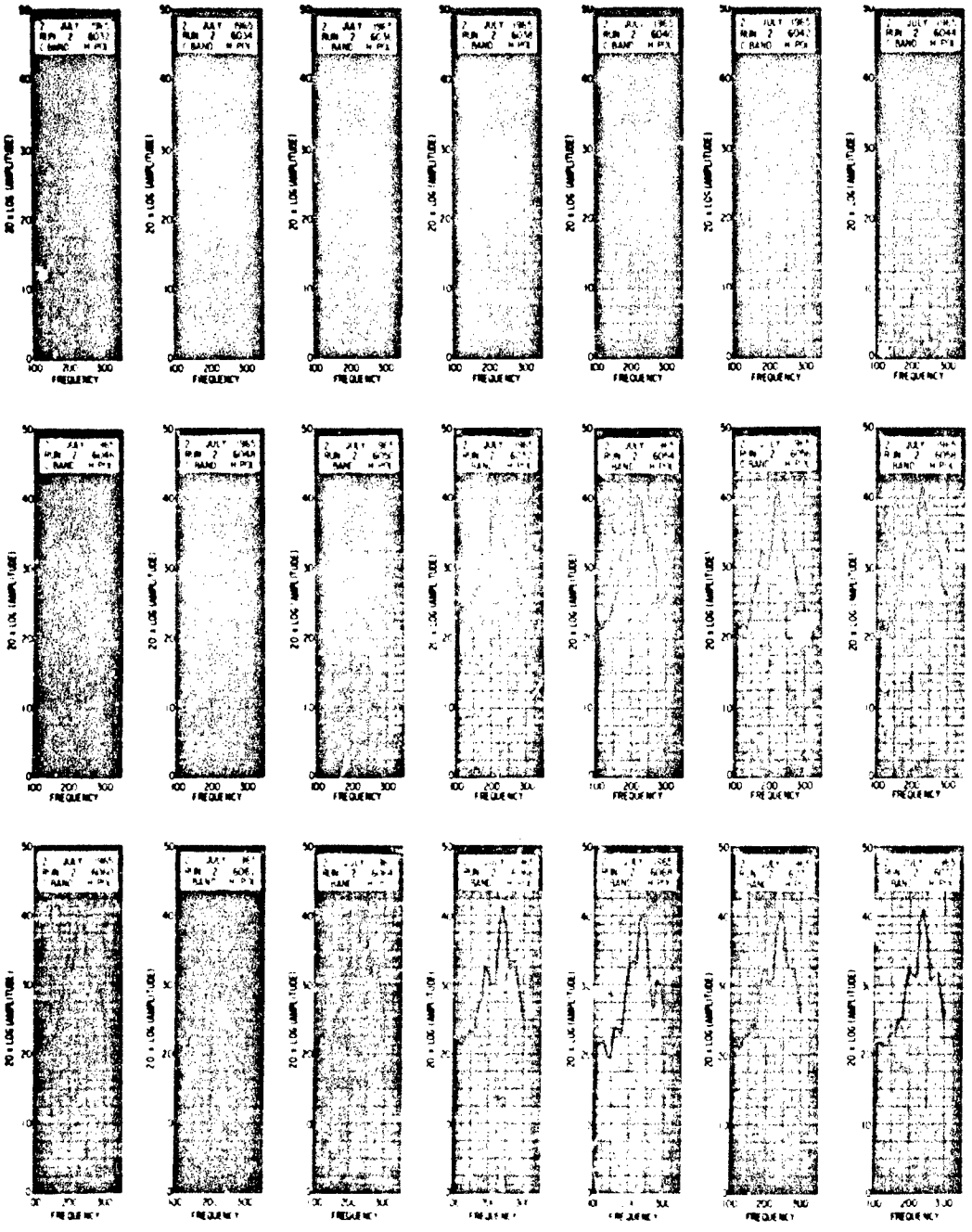

Fig. 26 - Clutter power spectra, July 2, 1965, run 2, C band, High resolution

Fig. 27 - Clutter power spectra, July 2, 1965, run 2,
C band, VV polarization

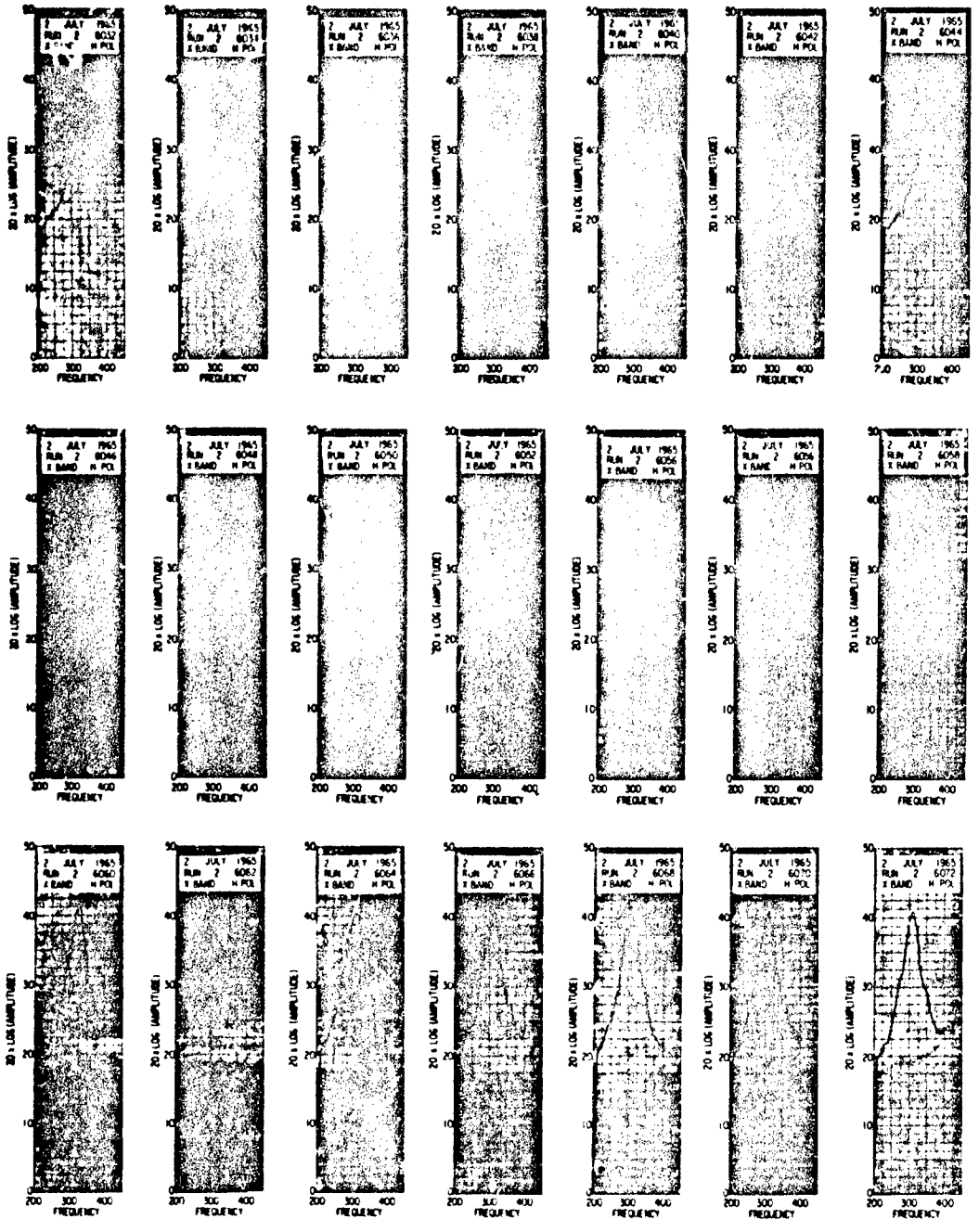

Fig. 28 - Clutter power spectra, July 2, 1965, run 2, X band, HH polarization

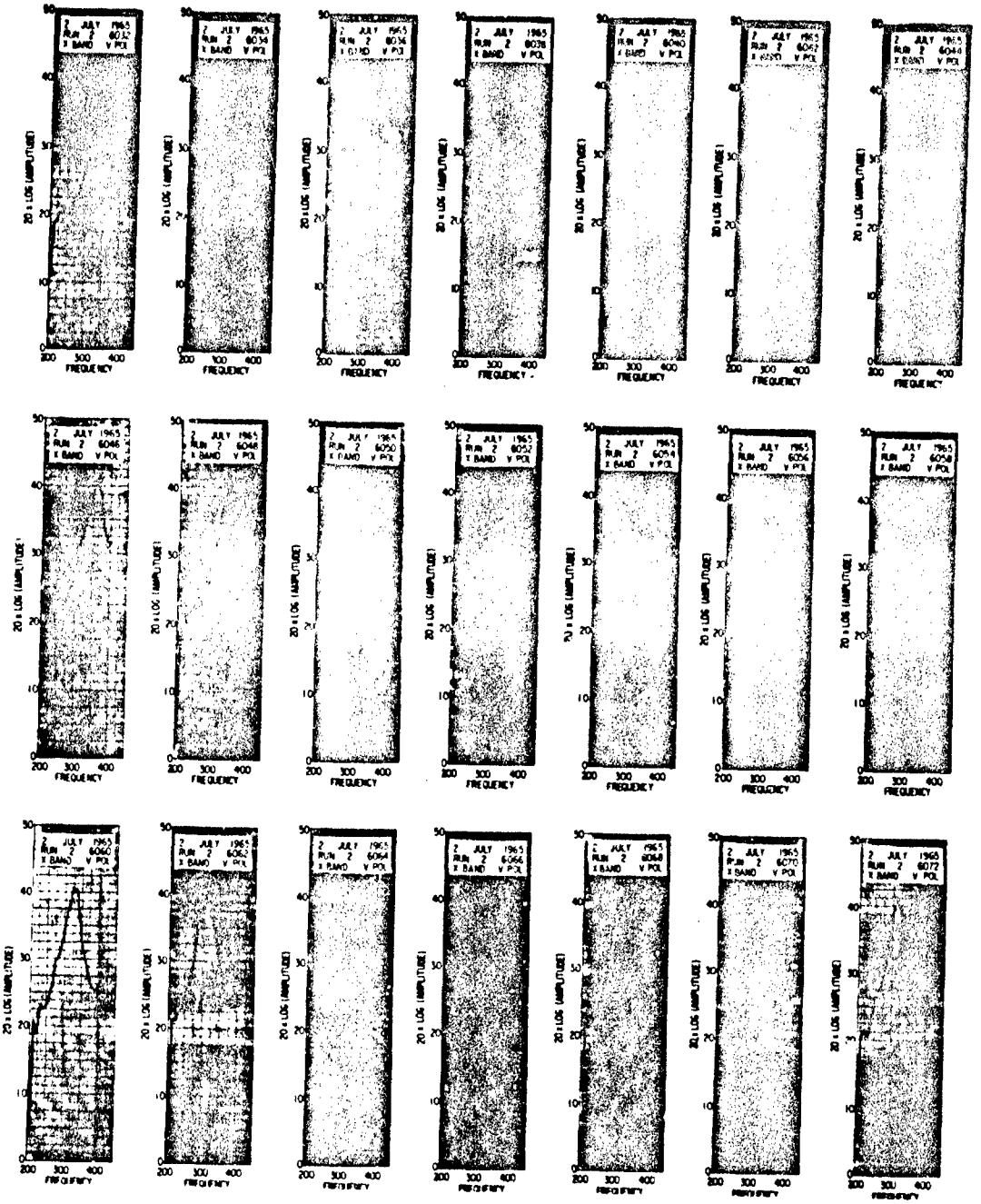

Fig. 29 - Clutter power spectra, July 2, 1965, run 2, X band, VV polarization

which are averaged to produce the plots are contiguous, however. Each plot is labeled with the run number, polarization transmit-receive combination, number of degrees of freedom in the average (number of individual graphs), the window width in cycles, the reference clock time on the tape recorder, the date of the run, the frequency transmitted, and the approximate geographic area. The frequency axis is the image (alias) axis, not the true doppler axis. The ordinate of the spectra is relative energy (amplitude squared). The Denver flight spectra (Figs. 21 through 28) have window widths of 10 cps for X- and C-band spectra, 5 cps for L-band spectra, and 2 cps for P-band spectra. These spectra are likewise averages containing 40 degrees of freedom in the X- and C-band spectra, 20 in L band, and eight in P band. These correspond to segment lengths of 0.05, 0.05, 0.1 and 0.25 second respectively for the individual spectra. In all, 42 seconds of data were analyzed, resulting in 21 spectra for each of the frequency-polarization pairs. The ordinate on these curves is decibels above the system noise level, which may be assumed to be between 85 and 90 dbm.

The pointing angles involved were elevation 4 degrees, azimuth 22 degrees for Eastern Shore, while for Denver they were 8 and 0 degrees. The aircraft velocity is a nominal 300 ft/sec.

Cancellation

A conventional delay-line canceller (9) utilizes a delay line of length T equal to the interpulse interval and a subtraction device to form the difference between successive pulses (single delay) or between successive pulse differences (double delay). If R_m is the amplitude of the first such pulse and R_n the amplitude of the second, then the average residue after cancellation of a number of such pairs is

$$E[(R_m - R_n)^2] = E[R_m^2] + E[R_n^2] - 2E[R_m R_n] \tag{19}$$

where E is the expectation operator. The cancellation ratio of a delay-line device is defined as

$$C_c = \frac{\text{clutter power in}}{\text{clutter power out}} = \frac{E[R^2]}{E[(R_m - R_n)^2]} \tag{20}$$

If $E(R_m^2) = E(R_n^2) = E(R^2)$, then combining Eqs. (19) and (20)

$$C_c = \frac{1}{2(1 - \rho_x(\tau))} \quad \text{where } \rho_x(\tau) = \frac{E(R_m R_n)}{E(R^2)} \tag{21}$$

and combining with Eq. (16),

$$C_c = \frac{1}{1 - f^2(\tau)} \tag{22}$$

Expanding (Ref. 7) $f^2(\tau)$ in terms of its moments, and assuming symmetry of the spectrum so that only even central moments need be considered,

$$f^2(\tau) = 1 - \tau^2 + \frac{\tau^4}{2!} - \cdots \tag{23}$$

And therefore for main-beam clutter,

$$C_c = \frac{1}{4(\pi\tau)^2 \mu_2^2} , \tag{24}$$

For a single delay-line canceller $\tau = T$, so that

$$C_c = \frac{f_r^2}{\sigma_c^2} \tag{25}$$

where σ_c^2 is the variance of the clutter spectrum in radians per second, and f_r is the pulse-repetition rate. To determine the effect of approximating $\chi^2(\tau)$ by its second moment along, a calculation was made using a cosine-squared approximation to the 4F radar X-band antenna with the feature that the side lobes are adjustable. The pattern was of the form:

$$\begin{aligned} G^2(\psi) &= G_0 \cos^2 (45/2\,\psi) \qquad -4^\circ \le \psi \le 4^\circ \\ G^2(\psi) &= \alpha' G_0 \sin^2 (45\phi) \qquad -8^\circ \le \psi \le -4^\circ \\ &\qquad\qquad 4^\circ \le \psi \le 8^\circ. \end{aligned} \tag{26}$$

Where G_0 is a normalizing constant. Since the antenna azimuth pattern is related to the spectrum of a pulsed radar by

$$G^2(\psi)\, d\psi = W(f)\, df , \tag{27}$$

Eq. (15) was solved with the aid of Eq. (11) for $\lambda = 0.11$ ft, $v = 300$ ft/sec, and $T = 1/1576$ second for $\chi^2(\tau)$ as a function of the side-lobe level α'. The result was converted to cancellation using Eq. (22). The result of this calculation is shown in Fig. 30. For side-lobe levels greater than 10 db below the main beam, the increase in cancellation is almost linear with decreasing side lobes. Consequently, care must be utilized in the calculation of the cancellation ratio from the main-beam clutter spectral width alone.

CONCLUSIONS

The NRL clutter study has, in the first phase of the work, accomplished its primary objective of measuring clutter cross sections at small angles of incidence over various American and Canadian terrains. Data have been collected on four frequencies and two polarizations. In addition, spectra have been measured at the various frequency-polarization combinations. In the process of the study, a software library of special programs has been developed for data processing, and more effective calibration procedures have been developed. Certain theoretical studies have been performed both to determine the accuracy of the data and to provide pertinent parameters for specific radar problems. No new theoretical concepts have been discovered; however, certain parameters whose nature has been hitherto assumed have been measured and presented. The data presented in this report are not considered a complete coverage of the clutter problem. Obviously, more variety of terrain-type studies are required; for example, such categories as wooded areas, plains, suburban areas, urban areas, mountains, and

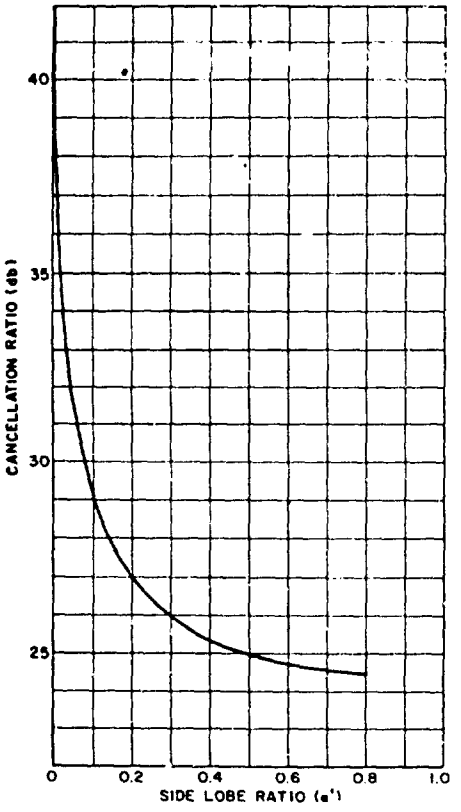

Fig. 30 - Effect of side-lobe level on cancellation

deserts. Transition areas, plains to mountains, land to sea, desert to mountains, etc., also have interest. In each of these instances, both distributions and spectra are required.

In the course of the study, several pertienent questions have arisen which require answers if radar performance is to be estimated. What, for example, is the effect, if any, of departure of the terrain-clutter distribution from the Rayleigh distribution, and what is the effect of the strong point scatterers on the various radar processing schemes? In general, the treatment of the entire area of the terrain effects on radar performance which, to date, has consisted of a single parameter to describe clutter power and an assumed spectral form given by the sandpaper model, which generally ignores terrain differences, is obviously inadequate to define the behavior of the more sophisticated systems presently under consideration. To fill this need for specific answers, an accurate and flexible clutter model is required which will contain not only the terrain characteristics but also the flexibility to include the parameters of the radar to be analyzed.

In this regard, it is necessary to define two general types of mathematical models, the rigid model and the statistical model. The rigid model consists of deterministic expressions obtained by physical analysis or by empirical curve fitting of data which, when combined with certain input parameters, yield a prediction of performance in terms of a set of output parameters of assigned value. A statistical model (dynamic model) consists of a series of probabilistic expressions derived from physical analysis

or from real data which, when combined with the input parameters, yield a statistical measure of the performance, and includes the rigid model as a special case. That is, the averages derived from the statistics should yield the rigid-model results, assuming sufficient averaging time is provided. Since the terrain seen by an airborne radar returns energy which fluctuates, both because of changes in the relative phasing of scattered signals and because of variations in terrain reflectivity, both of which are essentially statistical quantities, a model which is able to represent these quantities as data would seem superior. The implementation of such a model, while difficult, is not impossible.

In the course of this study, the concept of a statistical model based upon synthetic-aperture mapping has evolved. A synthetic-aperture map, or for that matter, PPI maps and scanning-aperture maps, are plots of terrain reflectivity (radar cross section per resolution cell) as a function of the range and distance along the flight path (azimuth for PPI). The photographic medium offers high storage capacity combined with extremely slight dependence upon the viewing radar. The parameters of primary interest are the viewing angle and resolution cell. So within these limits they are characteristic of the terrain alone. Such a map can be converted to data suitable for computer processing in a manner which preserves not only the relative values of reflectivity but also the spatial distribution by equipment already procured by NRL. The four-frequency radar system is being equipped with recorders to allow the synthetic-aperture technique to be applied to all signals supplied by this system.

Briefly, the radar maps will be quantized into areas equal to the resolution cell of the map by use of a microdensitometer whose output will be digitalized to provide both a measure of cross section and coordinates. The resulting information will be recorded on magnetic tape for computer entry. In the computer a model antenna will be moved over the terrain data, and each cross section will be assigned a random phase and summed within the illuminated area. As the radar proceeds over the terrain, the illuminated area will move over the model terrain, and thus a clutter signal as a function of time will be generated.

The major advantage of this technique is the close association between the clutter data and the geographical location of the scatterers. Correlations can be achieved which were beyond the elaborate program attempted with the Pisgah crater data described earlier in this report. The major disadvantage is the difficulty involved in calibrating a radar map. A more detailed analysis of this technique will be made in the course of the second phase of the study. It should be noted that the addition of the mapping equipment will in no way hinder the data collection facilities presently available.

In summary, the NRL clutter study has (a) cataloged data over a number of terrains concerning the radar cross section and fluctuation spectra, (b) presented analyses which demonstrate the existence of at least two processes in terrain clutter, the random Rayleigh-like clutter and the signal-plus-noise-type clutter, (c) proposed a statistical model based on synthetic aperture mapping which will enable the evaluation of the interaction of radar systems with specific terrain features.

REFERENCES

1. Bimonthly Report No. 1, AF MIPR AS-5-64, 18 Jan. 1965

2. Bimonthly Report No. 2, AF MIPR AS-5-64, 15 Jul. 1965

3. Bimonthly Report No. 3, AF MIPR AS-5-64, 19 Feb. 1966

4. Barlow, E.J., "Doppler Radar," Proc. IRE 37:340-355 (Apr. 1949)

5. Emerson, R.C., Rand Corporation, R-274, Mar. 1, 1954

6. Rice, S.O., "Mathematical Analysis of Random Noise," Bell System Tech. J. Vol. 23, p. 282, 1944 and Vol. 24, p. 46, 1945

7. McGinn, J.W., Jr., and Pike, E.W., "A study of Sea Clutter Spectra." in "Statistical Methods in Radio Wave Propagation," pp. 49-92, New York; Pergamon Press, 1960

8. Urkowitz, H., "An Extension to the Theory of the Performance of Airborne Moving-Target Indicators," Trans. IRE Vol. ANE-5, 210, 1958

9. Skolnik, M.I., "Introduction to Radar Systems," p. 113, New York; McGraw-Hill, 1962

Appendix A

THE FOUR-FREQUENCY RADAR SYSTEM

The four-frequency radar system is basically four different pulsed coherent radars transmitting at P band (428 Mc), L band (1225 Mc), C band (4455 Mc), and X band (8910 Mc). The transmitted signals are generated at a low level by a stable signal source which utilizes a 1.15 Mc precision oven-controlled Manson basic oscillator, varactors, and transistors to provide multiplication and signal amplification to the desired frequency ranges. In addition to the transmission frequencies, a 37-Mc reference frequency is provided for use in coherent detection. The outputs of the stable signal source (30 mw) are fed to their respective transmitters and amplified to the final output levels. Two types of coherent transmitter chains are used, namely, tetrodes in external coaxial cavities for P and L bands, and one or two TWTs (rf pulsed) driving klystron power amplifiers for C and X bands. At P and L bands, in order to obtain adequate bandwidth, the driver stages are operated cw and the output stage is pulsed with switch tubes to provide the desired rise times.

Each of the four radars is designed to operate with two antennas, one polarized horizontally and one vertically, either separately or pulsed alternately. The four frequencies can be transmitted singly or pulsed in rapid succession to provide a total of eight different frequency-polarization combinations. The basic timing for the system is provided by the synchronizer and ranging unit. It supplies modulator triggers, video pulse drives, sweep triggers, timing marks, pulse-repetition frequencies, pulse widths, and gate widths. The reference used for this unit is an 82-kc clock which is counted down to the desired rates. In each radar, an antenna switch controlled by the synchronizer switches the transmitter output pulses alternately between the duplexer systems of the two antennas, horizontal and vertical, associated with a given frequency transmission.

The four-frequency antenna system consists of two pairs of antennas located back to back on a common mount. One pair contains the lower-frequency antennas, P and L, which are crossed dipoles with a common ground plane. The second pair contains the C- and X-band antennas, which have separate parabolas facing 180 degrees away from the dipole arrays. The antennas can be rotated through 315 degrees of azimuth and 100 degrees of elevation, and are stabilized in roll and pitch with reference to magnetic north and vertical. They are capable of being sector scanned at 30 degrees per second. The antenna is mounted in a radome on the underside of the aircraft.

On reception, the signals from the horizontal and vertical antennas are passed through their respective duplexers to the two microwave mixers and preamplifier units, where they are converted to i-f frequency (37 Mc) and amplified. Each of the eight (two per frequency) i-f preamplifiers has a conventional Wallman cascade input circuit, followed by a buffer tube and a beam-deflection tube switch to time share the common horizontal and vertical i-f receiving channels. The horizontal or vertical i-f receiving channels are identical, and each consists of parallel i-f amplifiers, one limiting and one logarithmic. The logarithmic amplifier has a bandwidth of 12 Mc, a lin-log transfer characteristic linear within 0.5 db over 45 db of dynamic range, and performance independent of overall radar duty-cycle variations of 600 to 1. The limiting amplifier is designed to produce minimum phase error over a large range of input-amplitude variation. The amplifier uses a Z-2800 beam-deflection tube which has excellent limiting

characteristics, constant input and output characteristics, and insignificant input-output coupling. Measurements on this amplifier have shown an output variation of a small fraction of a decibel for 70 decibels of input range. The phase variation was within ±2. 5 degrees for 60 db of input range.

Two forms of second detection are used. The logarithmic amplifier has a detector with a square-law characteristic, while the limiting amplifier has a linear synchronous detector using the 37-Mc signal from the stable signal source as reference. An additional phase detector is included which allows the phase difference between the horizontal and vertical signals to be measured. Consequently, five video outputs are available for recording for each transmitted frequency, namely, the amplitudes of the direct and cross polarized return, their phases with respect to the 37-Mc reference, and their phase with respect to each other: these outputs are capable of being displayed on A scopes for the purpose of selecting a range at which the signal is to be recorded. Two range gates may be used: the main range gate which may be set with an accuracy of several yards out to maximum range and an auxiliary gate which may be positioned with respect to the first. Digital readout to the nearest yard is provided for the main range gate.

Finally, a 16-head, one-inch magnetic tape system is used for data recording. The maximum data rate is 25, 600 seven-bit binary words per second. Each of these words is the amplitude existing instantaneously at the detector outputs at the time of the range gate. These amplitudes are digitalized in groups of four, since four amplitudes are available for each pulse transmitted. In addition to these high-rate signals, ten other slowly varying parameters may be recorded, one every second. Tables A1, A2, and A3 give a listing of the characteristics of the system which has been outlined and give a graphic presentation of the extreme flexibility embodied in the four-frequency radar.

Table A1
Principal Parameters of Four-Frequency Radar System - Transmitters

Parameter	Frequencies			
	428 Mc	1225 Mc	4455 Mc	8910 Mc
Long-term frequency stability - no greater than	1 part in 10^6 per day	1 part in 10^6 per day	1 part in 10^6 per day	1 part in 10^6 per day
Short-term frequency stability (0. 01 sec)	Within 5 parts in 10^9 - 10^8	Within 5 parts in 10^9 - 10^8	Within 5 parts in 10^9 - 10^8	Within 5 parts in 10^9 - 10^8
Peak power	35-40 kw	35-40 kw	25 kw	40 kw
Average power	140 watts	140 watts	100 watts	160 watts
Peak power special mode	10 watts	10 watts	10 watts	10 watts
Interpulse phase stability no greater than	4°	4°	5°	6°
Output Tube	7651 tetrode (RCA)	7651 tetrode (RCA)	SAC - 290 Klystron (Sperry)	V24C Klystron (Varian)

Table A2
Principal Features of Four-Frequency Radar System - Signal and Display Parameters

Parameter	Value
Repetition rates	Submultiples of 81.959 kc: 100.45, 200.90, 301.35, 394.07, 512.30, 602.71, 683.07, 788.16, 1463, 2926 cps.
Pulse widths	0.1, 0.25, 0.5, 1, 2 μsec
Noise figure	9-11 including all rf losses
I-F amplifier Center frequency Bandwidth Type Quantity	 37 Mc 10, 4, 2, 1, 0.5 Mc lin-log, 25 and 50 db dynamic range Limiting Two - One for horizontally polarized signals, one for vertically polarized signals.
Range gate Width Increment readout	 0.1, 0.2, 0.5, 1, 3, 5 μsec 1 yard
Range marks Width Spacing	 1.0, 2.0, 5.0, 20 μsec 1, 5, 20 nautical miles
Video system Consoles Displays CRT size	 Total 3: 2 operators and 1 master control Dual-beam A scope, B scope and PPI for each console. All flat face tubes. 5 in.
Signal outputs (ungated and gated)	Vertical polarization signal amplitude Horizontal polarization signal amplitude Vertical/horizontal polarization phase Horizontal polarization/transmitted signal phase Vertical polarization/transmitted signal phase
Maximum Video Amplitude	2 volts, peak-positive

Table A3
Project Suspender Antenna System Performance

Parameter	P-Band		L-Band		C-Band		X-Band	
Polarization	Horiz.	Vert.	Horiz.	Vert.	Horiz.	Vert.	Horiz.	Vert.
Bandwidth (Mc)	± 5	± 5	± 5	± 5	±10	±10	±10	±10
Azimuth beamwidth (degrees)	12.3	12.1	5.5	5.5	5	5	5	4.7
Elevation beamwidth (degrees)	40	41	13.8	13	5	5	5.3	5
Azimuth minor lobe (db)	14.5	14.5	13.4	14	23.2	23.0	23.6	23.6
Elevation minor lobe (db)	30	26	16	14	24.5	24	23.5	24.2
Cross polarization (db)	25	28	25	25	>20	>20	>20	>20
Transmission line loss (db)	0.6	0.3	0.6	0.8	2.0	2.0	0.6	0.6
Antenna gain (db)	17.4	17.4	25.9	26.2	31.4	31.4	31.2	31.2
Voltage standing-wave ratio	<1.44:1	<1.38:1	<1.35:1	<1.28:1	<1.50	<1.57	<1.30:1	1.12:1
High power	OK	OK	OK	OK	Not Measured		OK	OK

Appendix B

SYSTEM CALIBRATION AND SOURCES OF ERROR

Two measurements are required for an absolute system calibration: (a) a measurement of the receiver linearity and gain, and (b) an absolute power measurement independent of the system. The receiver gain and linearity measurements were made using an external signal generator and variable precision attenuators. In addition, a re-entrant test signal generated within the system is monitored during the data-collection runs to provide a check of receiver stability. Calibrations were thus obtained for each transmitted frequency polarization signal.

Absolute power measurements were obtained by tracking an eight-inch-diameter aluminum sphere dropped from the plane. The sphere is weighted to fall at a constant angle relative to the antenna. The magnitude of the sphere return is recorded and the range logged. Applying the radar equation to the sphere return denoted by the subscript(s) yields

$$S_s = \frac{(4\pi)^3}{G^2 \lambda^2} \frac{P_{rs}}{P_{TS}} R_s^4 \cdot \tag{B1}$$

For the terrain measurement, the radar equation becomes

$$S_T = \frac{(4\pi)^3}{G^2 \lambda^2} \frac{P_{rt}}{P_{Tt}} R_T^4 \cdot \tag{B2}$$

The ratio of Eq. (B2) to Eq. (B1) yields

$$S_T = \frac{P_{RT}}{P_{RS}} \left(\frac{R_T}{R_S}\right)^4 S_S \tag{B3}$$

where the peak transmitted power is the same for both measurements. Since all other quantities are measured, the terrain cross section becomes a function of the returned signal, P_{RT}.

There are two basic errors in this calibration system: (a) receiver stability, and (b) tracking error in the sphere measurement. Previous data have shown that the sphere measurement has an error of approximately 0 to 2 db, due chiefly to the variation of the position of the sphere within the beam. This error is minimized by measuring several spheres for each calibration and using the strongest return at a given range. The receiver stability is monitored, as stated previously, by recording a known reference level at various time intervals. The reference has an uncertainty of approximately 1 db for all frequencies and polarizations.

Consequently, for any given value of cross section a maximum error of ±3 db is possible. However, the polarization ratio would contain only the stability error, since

the tracking error is common. Frequency ratios of X to C band or L to P band would likewise have only stability errors, since the sphere is illuminated by these frequencies simultaneously.

The above analysis does not take into account all possible sources of error, such as variations in transmitter power, antenna isolation, receiver crosstalk, etc. These errors are negligible except where specifically mentioned. Since the received signal is measured with respect to a sphere, and since all frequencies and polarizations are calibrated with the sphere data, comparisons between any two components will contain errors principally due to the two factors discussed previously.

Appendix C

DATA PROCESSING

In order to determine the Doppler (clutter) spectrum from the phase-versus-time samples, two approaches are possible - the indirect approach, in which the autocorrelation function of the data is first determined and the power spectrum derived from its cosine transform, and the direct approach, in which the complex amplitude function of the data is determined and the power spectrum derived from its square. The latter approach was chosen, since it offers more flexibility in the choice of analysis bandwidth and frequency resolution and allows effective monitoring of the spectral position.

For data which are periodically sampled at a rate f_r, the pulse-repetition rate, which produces a time spacing between samples of ΔT, the Fourier coefficients $a(f)$ and $b(f)$ are given by:

$$a(f) = \frac{1}{N} \sum_{n=0}^{N} X(n\Delta T) W(n\Delta T) \cos 2\pi f(n\Delta T)$$

$$b(f) = \frac{1}{N} \sum_{n=0}^{N} X(n\Delta T) W(n\Delta T) \sin 2\pi f(n\Delta T) \qquad \text{(C1)}$$

where N is the number of points in a sample, $X(n\Delta T)$ is the series of phase points, and $W(n\Delta T)$ is the sampling function. Several choices of sampling function are available; however, in view of the quantities of data to be processed, a sampling function which optimizes program speed was chosen, namely:

$$W(nT) = 1 \qquad n = N$$

$$0 \qquad \text{otherwise.} \qquad \text{(C2)}$$

The analysis window established by this function is given by its Fourier transform:

$$H(f) = \frac{1}{T_m} \int_0^{T_m} W(t) e^{-j2\pi ft}\, dt. \qquad \text{(C3)}$$

from which the power transfer function becomes:

$$|H(f)|^2 = \frac{\sin^2 \pi f T_m}{(\pi f T_m)^2} \qquad T_m = N\Delta T \qquad \text{(C4)}$$

where T_m is the length of the sample. The equivalent width of the filter between zeroes is then:

$$B = \frac{1}{2T_m} \qquad \text{(C5)}$$

This relationship between the window width (equivalent analog filter width) and the sample length allows the resolution of the spectrum to be controlled simply.

The estimate of the energy in the spectrum at frequency f is given by:

$$A^2(f) = a^2(f) + b^2(f) \tag{C6}$$

and the estimate of the total power in the spectrum for a sample length T_m is given by:

$$P(f, T_m) \sim 2 \int_0^{1/2\, f_r} A^2(f)\, df \,. \tag{C7}$$

The proportionality exists since the spectrum is uncalibrated, while the factor 2 is included since both positive and negative frequencies contribute to the integral. The total power in the present system is a constant, since the limiter provides a constant-input amplitude to the phase detector, while the phase between the reference oscillator and the signal is sufficiently variable to average to a constant multiplying factor. This system characteristic may be used to check the accuracy of the computation. The total power $P(f, 10\,T_m)$ was computed for each of the spectra of the X-band return (HH polarization) of run 57, Eastern Shore, Maryland and for an equal number of spectra of the C-band return (VV polarization) of the same run. The percentage deviation from the mean was 5 percent for the X-band power and 9 percent for the C-band power. These results were considered quite satisfactory, since only the portion of the spectra containing clutter energy was used in the computation. This portion amounted to approximately 50 percent of the ranges from 0 to $1/2\, f_r$ for X-band and 25 percent of the range for C-band. The inclusion of the system noise included in the remainder of the range would lessen the percentage deviation considerably.

A second test of the accuracy of the data is based on the limiting form of the clutter spectrum. The limiting form may be determined for the case of an antenna whose two-way power pattern is $G^2(\theta)$ which is modulated by any terrain cross section which is independent of θ in the sampling interval and which has a distribution given by:

$$P(S) = \frac{1}{S_0}\, e^{-S/S_0} \quad S > 0 \,. \tag{C8}$$

The limiting form of the clutter spectrum becomes:

$$S(\theta) \int_0^{\infty} SP(S)\, G^2(\theta)\, dS = S_0 G^2(\theta) \tag{C9}$$

$$S(f) = S_0 G^2(f) \tag{C10}$$

where the angle axis of the power pattern has been converted to a frequency axis by the transformation:

$$\theta = \cos^{-1} f/f_0 \,. \tag{C11}$$

Equation (C10) states that the limiting form of the clutter spectrum should be similar in shape to the antenna power pattern. This relation was verified by averaging consecutive spectra and comparing the average with the antenna power pattern converted to frequency abscissa. The power pattern was fitted to the data by multiplying it by an arbitrary constant and adding a correction for system noise. The closeness of the fit is shown by Figs. C1 through C4.

Considerable discussion has arisen in the past few months concerning the effect on the clutter spectrum of the hard limiting which precedes phase detection. In general, hard limiting produces harmonic distortion of the limited signal. In the present system, hard limiting occurs at i-f and is followed by a bandpass filter centered at the i-f (37 Mc). The phase distortion due to limiting is approximately 5 degrees of phase over the whole amplitude range. That is, the phase of an input signal is measured to this accuracy independently of its amplitude. The pertinent question (aside from the effect of the 5 degree errors) then is how much information is common to the phase spectrum, the amplitude spectrum, or a mixture of the two. McGinn and Pike (7) give all of the relationships that they could find for narrow-band noise-type signals and point out (page 67) that the second-probability densities of amplitude and phase are functions of the same single variable:

$$Z^2(t) = \left[\int_{-\infty}^{\infty} a(f)\cos 2\pi f\tau\, df\right]^2 + \left[\int_{-\infty}^{\infty} a(f)\sin 2\pi f\tau\, df\right]^2 \qquad \text{(C12)}$$

which is very nearly (page 70) the autocorrelation of the signal amplitudes. The phase and amplitudes are well correlated, but the author knows of no analysis of what types of signal fluctuations are not common to the two spectra. This correlation has been empirically demonstrated by side-looking mappers which are usually greatly limited, yet produce terrain maps which are in effect plots of terrain cross section versus planar coordinates. As a result of these arguments, the spectra presented in this report are an accurate measure of the phase spectrum and highly correlated with the amplitude spectrum.

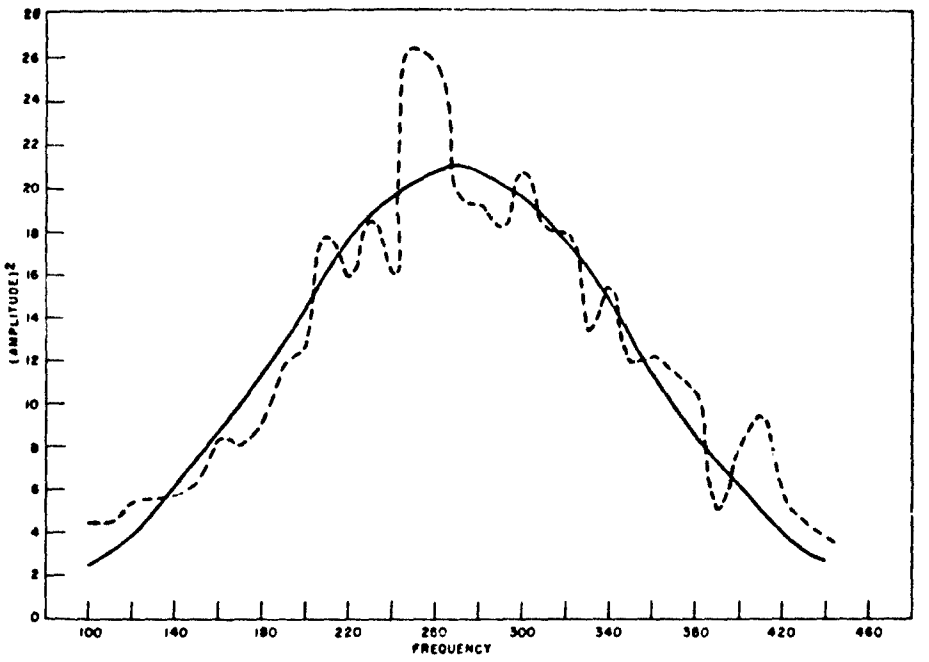

Fig. C1 - Average spectrum, Dec. 10, 1964, time 19013, run 57, Eastern Shore, Md., X band, HH polarization, 10 degrees of freedom, 10 cps bandwidth

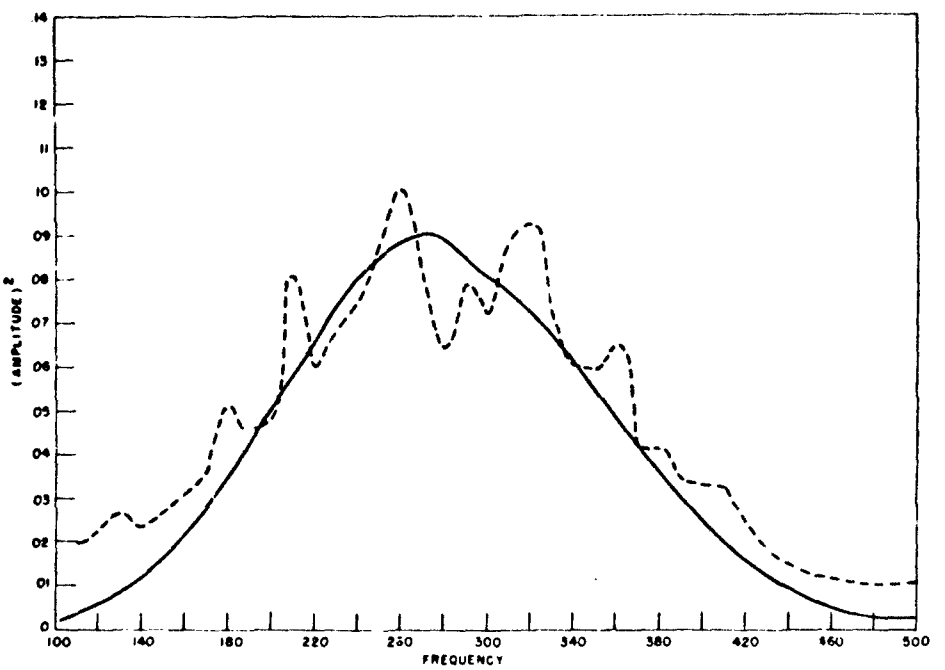

Fig. C2 - Average spectrum, run 57, Dec. 10, 1964, time 19013, Eastern Shore, Md., X band, VV polarization, 10 degrees of freedom, 10 cps bandwidth

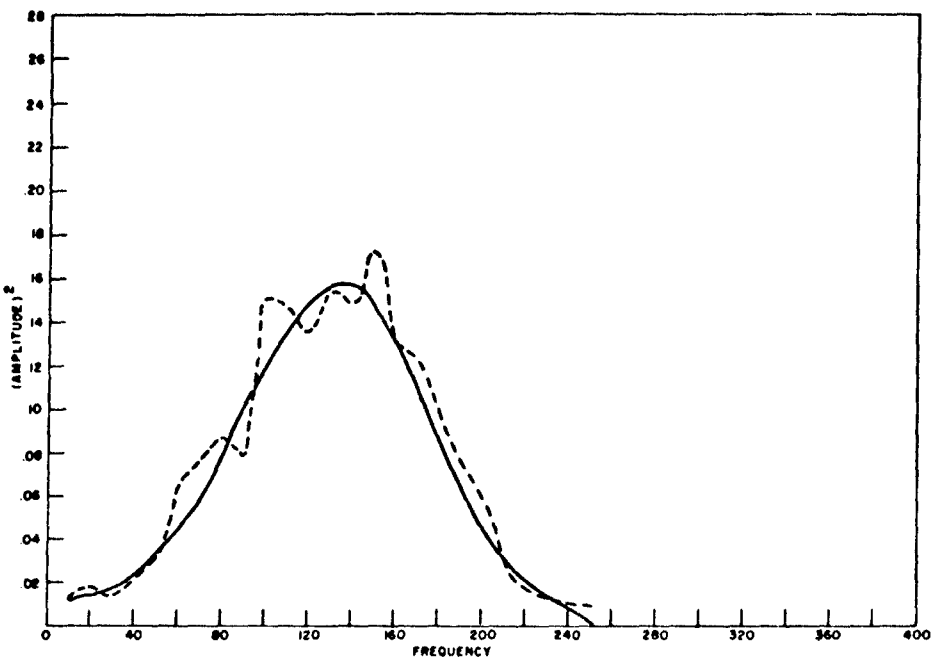

Fig. C3 - Average spectrum, run 57, Dec. 10, 1964, time 19013, Eastern Shore, Md., C band, HH polarization, 10 degrees of freedom, 5 cps bandwidth

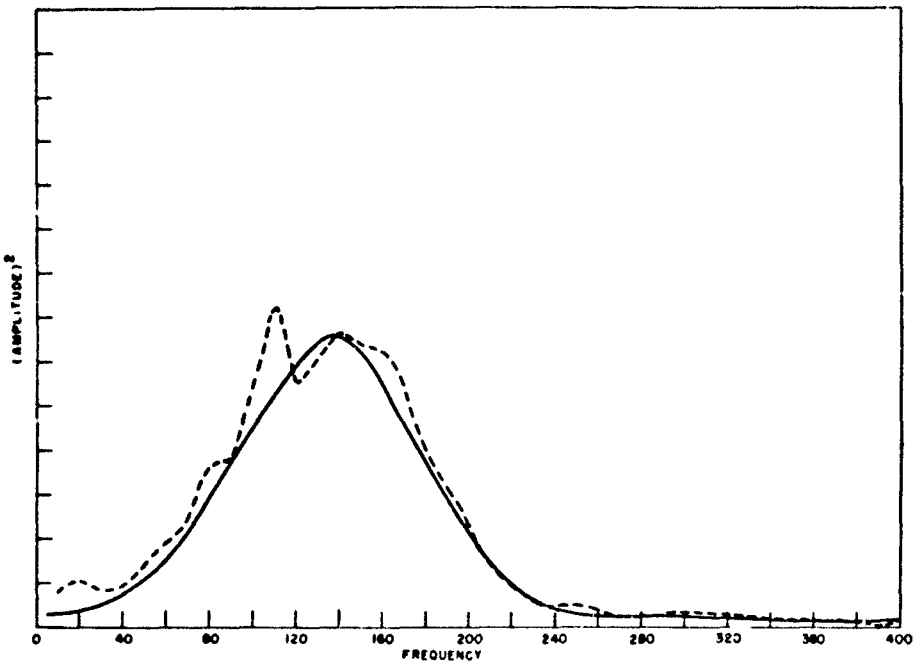

Fig. C4 - Average spectrum, run 57, Dec. 10, 1964, time 19013, Eastern Shore, Md., C band, VV polarization, 10 degrees of freedom, 5 cps bandwidth

Security Classification

DOCUMENT CONTROL DATA - R & D

Security classification of title, body of abstract and indexing annotation must be entered when the overall report is classified)

1 ORIGINATING ACTIVITY (Corporate author) Naval Research Laboratory Washington, D. C. 20390	2a. REPORT SECURITY CLASSIFICATION Unclassified 2b GROUP

3 REPORT TITLE

NRL TERRAIN CLUTTER STUDY, PHASE I

4 DESCRIPTIVE NOTES (*Type of report and inclusive dates*)

An interim report on the problem

5 AUTHOR(S) (*First name, middle initial, last name*)

Norman W. Guinard, John T. Ransone, Jr., Michael B. Laing, and Lenard E. Hearton

6 REPORT DATE	7a. TOTAL NO OF PAGES	7b NO OF REFS
May 10, 1967	64	9

8a CONTRACT OR GRANT NO NRL Problem R07-02 b. PROJECT NO MIPR AS-5-64 c. d	9a. ORIGINATOR'S REPORT NUMBER(S) NRL Report 6487 9b. OTHER REPORT NO(S) (*Any other numbers that may be assigned this report*)

10 DISTRIBUTION STATEMENT

Distribution of this report is unlimited.

11 SUPPLEMENTARY NOTES	12 SPONSORING MILITARY ACTIVITY Department of the Air Force (Systems Engineering Group, SEAFW) Wright-Patterson Air Force Base

13 ABSTRACT

The first phase of a terrain-clutter study has been completed at NRL, utilizing the four-frequency radar system installed in a WV2-128324 (Super Constellation) aircraft. This system is capable of transmitting and receiving four frequencies (P, L, C, and X) consecutively with a choice of horizontal, vertical, and alternating polarizations. The returns are gated at a fixed range and analyzed in a digital computer. Absolute clutter measurements have been taken over both Canadian and American sites at angles of incidence of 10 degrees or less. Two parameters have been measured. The first is the normalized radar cross section in terms of the 10, 50 (median), and 90 percentile values of its distribution, while the second is the fluctuation power spectrum of the coherent radar return signal. Two types of statistical processes have been determined from the cross-section data; one follows a Rayleigh distribution between 10 and 90 percentile values, and one departs radically from this distribution. The energy in the fluctuation power spectrum has been estimated in frequency bands whose spacing is determined by the transmitted frequency, e. g., 2 cps at P band through 10 cps at X band. The root mean square deviations of the estimates indicate likewise a Rayleigh behavior for certain bands and a radical departure from this behavior. In this case, the radical departure is identified as a Ricean (signal plus noise) distribution produced by strongly reflecting point targets in the illuminated area. A statistical model for terrain clutter is proposed which will enable the

(Abstract continues)

DD FORM 1 NOV 65 1473 (PAGE 1)

S/N 0101-807-6801

Security Classification

Security Classification

14 KEY WORDS	LINK A		LINK B		LINK C	
	ROLE	WT	ROLE	WT	ROLE	WT
Radar Research Terrain Clutter Surface effects Detection Background noise Scatter Backscatter Normalized cross section data Four-frequency radar system X, C, L, P frequency data						

phenomenon disclosed by the study to be simulated based upon the optical analysis of Synthetic Aperture Radar Maps.

DD FORM 1 NOV 1473 (BACK)
(PAGE 2)

Security Classification